AFIT/GA/ENY/91D-6

STATIC PRESSURE MEASUREMENTS OF A LOW POWER ARCJET

THESIS

Kevin P. Talley, Captain USAF

AFIT/GA/ENY/91D-6

DISCLAIMER NOTICE

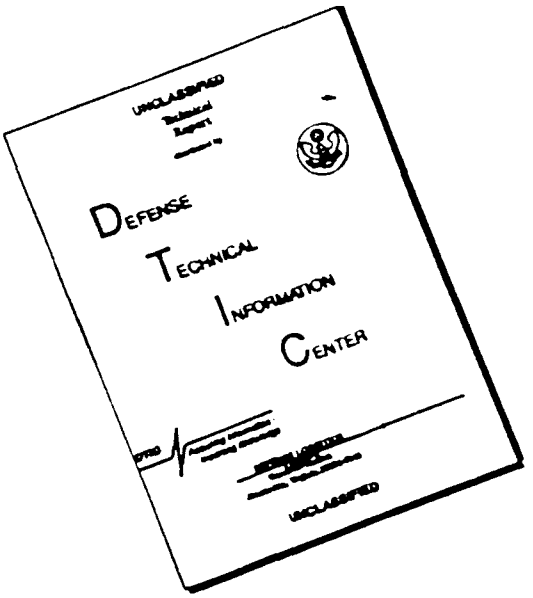

THIS DOCUMENT IS BEST QUALITY AVAILABLE. THE COPY FURNISHED TO DTIC CONTAINED A SIGNIFICANT NUMBER OF PAGES WHICH DO NOT REPRODUCE LEGIBLY.

AFIT/GA/ENY/91D-6

STATIC PRESSURE MEASUREMENTS OF A LOW POWER ARCJET

THESIS

Presented to the Faculty of the School of Engineering

of the Air Force Institute of Technology

Air University

In Partial Fulfillment of the

Requirements for the Degree of

Master of Science in Astronautical Engineering

Kevin P. Talley, S.B.

Captain, USAF

December 1991

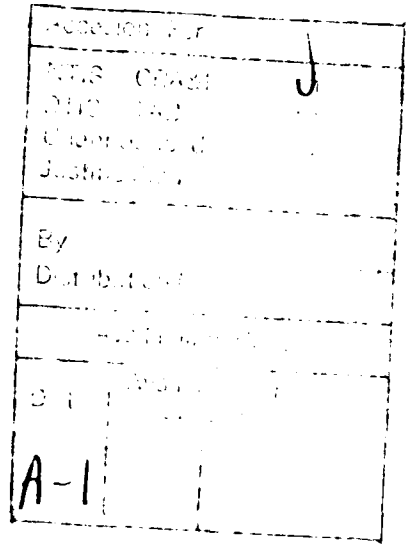

Approved for public release; distribution unlimited

REPORT DOCUMENTATION PAGE

Form Approved
OMB No 0704-0188

1. AGENCY USE ONLY (Leave blank)	2. REPORT DATE	3. REPORT TYPE AND DATES COVERED
	December 1991	Master's Thesis

4. TITLE AND SUBTITLE

STATIC PRESSURE MEASUREMENTS OF A LOW POWER ARCJET

5. FUNDING NUMBERS

6. AUTHOR(S)

Kevin P. Talley, Captain, USAF

7. PERFORMING ORGANIZATION NAME(S) AND ADDRESS(ES)

Air Force Institute or Technology, WPAFB OH 45433-6583

8. PERFORMING ORGANIZATION REPORT NUMBER

AFIT/GA/ENY/91D-6

9. SPONSORING / MONITORING AGENCY NAME(S) AND ADDRESS(ES)

Frank M Curran, SPTD-1
NASA Lewis Research Center
21000 Brookpark Rd.
Cleveland, OH 44135

10. SPONSORING / MONITORING AGENCY REPORT NUMBER

11. SUPPLEMENTARY NOTES

12a. DISTRIBUTION / AVAILABILITY STATEMENT

Approved for public release; distribution unlimited

12b. DISTRIBUTION CODE

13. ABSTRACT *(Maximum 200 words)*

The NASA Lewis 1.2 kilowatt arcjet has been used for a number of performance and lifetime studies. This design was modified to obtain static pressure measurements at several locations along the arcjet nozzle. These measurements were taken at various propellant flow rates over most of the operational envelope of the thruster. Measured static pressure distributions are considerably higher than predicted by ID models and are proportional to the arc power. A simple thermodynamic model is also compared to the data, and is shown to match the slope of the data while overpredicting the pressure.

14. SUBJECT TERMS

Electric Propulsion, Arcjet, Nozzle, Static Pressure

15. NUMBER OF PAGES

98

16. PRICE CODE

17. SECURITY CLASSIFICATION OF REPORT	18. SECURITY CLASSIFICATION OF THIS PAGE	19. SECURITY CLASSIFICATION OF ABSTRACT	20. LIMITATION OF ABSTRACT
Unclassified	Unclassified	Unclassified	UL

Acknowledgements

This document is based on a very "hardware intensive" experiment. The limited availability of the facilities needed to conduct this research meant an extended trip to NASA Lewis in Cleveland, Ohio, a journey which was both expensive and difficult to set up. I'd like to thank everyone who provided help and support in arranging that trip, especially W.C. Elrod, who told me of the possibility, Dave Byers, whose idea it was, Karen Criner and Frank Curran, who jumped through a lot of bureaucratic hoops on my behalf, and Docie Bailey, who processed my TDY orders at the last minute.

There were a lot of people at NASA whose assistance was invaluable. The engineers on the arcjet team were all helpful to me at one time or another, but I'd like especially to thank Frank Curran, John Sankovic, Charles Sarmiento, and Earl Morren. This project could never have happened without them. Members of the technical support staff who were especially helpful were Fred Jent, Jerry Schneider, Jerry Hill, and Mike Schaffner. They're part of the best tech staff I've ever worked with.

Finally, I'd like to thank my wife Clea, who let me go to Cleveland in the first place, and without whose love, prayer, and support I would have never emerged sane from this process.

Table of Contents

List of Figures

List of Tables

List of Symbols

A	cross sectional area	Z	compressibility
A^*	empirical constant, 120 Amps/cm^2-K^2	γ	ratio of specific heats
A	Amperes	Δh_f	specific heat of formation
c	effective exhaust velocity m/sec	ΔV	mission characteristic change in velocity
C_p	specific heat, J/kg-K	ϕ	work function, ergs
F	measured thrust, N	ρ	density, kg/m^3
g_0	gravitational acceleration m/sec^2	θ_{vib}	characteristic vibrational temperature
h	specific enthalpy, J/kg-K	η	efficiency
I_{sp}	specific impulse, secs	Subscripts	
j	current density, A/cm^2	0	stagnation condition
k	Boltzmann's constant	1	cold condition
M	Mach number	2	operational or hot condition
P	pressure	jet	kinetic power
R	gas constant, J/kg-K	arc	electrical power
T	temperature	c	chamber condition
W	power		

I Introduction

Spacecraft remain useful only as long as they have propellant. Onboard propellant is used not only to get a satellite to its desired orbit, but to keep it there as well. Space missions can be characterized by the amount of the velocity change, or ΔV, needed both to reach and to maintain the desired orbit. The amount of propellant necessary to give the desired ΔV is related spacecraft mass and engine performance by the Tsiolkovsky equation[1]

$$\frac{M_f}{M_o} = e^{-\frac{\Delta V}{c}} \tag{1}$$

where M_f is the spacecraft mass after engine operation, M_0 is the initial mass, and c is the effective exhaust velocity of the propellant gas. The exhaust velocity can also be expressed as

$$c = g_o I_{sp} \tag{2}$$

where g_0 is the acceleration of gravity and I_{sp} is the specific impulse. Stated simply, specific impulse is the duration (in seconds) that one pound of propellant will yield one pound of thrust for a given rocket engine. From the Tsiolkovsky equation, it is clear that the mass of propellant required for a given ΔV is greatly influenced by

the specific impulse--the higher the I_{sp}, the less propellant required. Conversely, for a fixed amount of propellant, even small changes in I_{sp} can have significant effects on the amount of available ΔV. For orbit transfer missions, higher I_{sp} means larger delivery capabilities to the target orbit, while for stationkeeping missions it can add years to the overall satellite lifetime.

For ideal, one dimensional nozzle flow, completely expanded, c can be given by[2]

$$c = I_{sp} g_o = \sqrt{2(h_c)} \qquad (3)$$

where h_c is the chamber enthalpy in the engine. Unfortunately, for chemical rockets the enthalpy is limited by the energy released by the propellants as they react. For the H_2-O_2 combination, the maximum I_{sp} is around 450 seconds. When the mission is limited to storable propellants such as hydrazine, this drops to 170-290 seconds[3].

Electric propulsion offers one way to exceed these limits. The energy for propulsion does not come from the propellants exclusively but additional power is added to them from an external source. There are three main ways to do this. Ion engines operate by first ionizing the gas and then accelerating the resulting ions with a high voltage grid. Magnetoplasmadynamic thrusters, on the other hand, use the electromagnetic forces resulting from a high power current discharge to propel the gas. The simplest approach,

however, is to heat the gas electrically and obtain thrust by expelling it out of a nozzle. This is known as electrothermal propulsion, and there are two major devices which fall into this category. One is the resistojet, where the gas is heated by means of a resistive heating element. These offer modest gains in performance but suffer from the limit imposed by the melting point of available refractory metals. Arcjets, the second major type of electrothermal thrusters, get around this by using an electric arc to heat the gas, the hottest core of which need not come into contact with the walls of the thruster (see Figure 1). This raises the attainable I_{sp} considerably.

Arcjets were studied extensively in the 1950's and '60's, Thirty kilowatt thrusters demonstrated I_{sp}'s up to 1500 seconds and efficiencies of around 40 percent[1]. Research trailed off after that, however, when it became evident that neither the missions nor the power supplies were likely to be developed in the near future. Research resumed in the early 1980's for two reasons: solar arrays large enough to deliver 30 kW were on the drawing board and power available on commercial communications satellites had become large enough that low power arcjet thrusters could be considered for stationkeeping.

Low power arcjet research has demonstrated lifetimes of over 1000 hours with performance in the 500 second region[3]

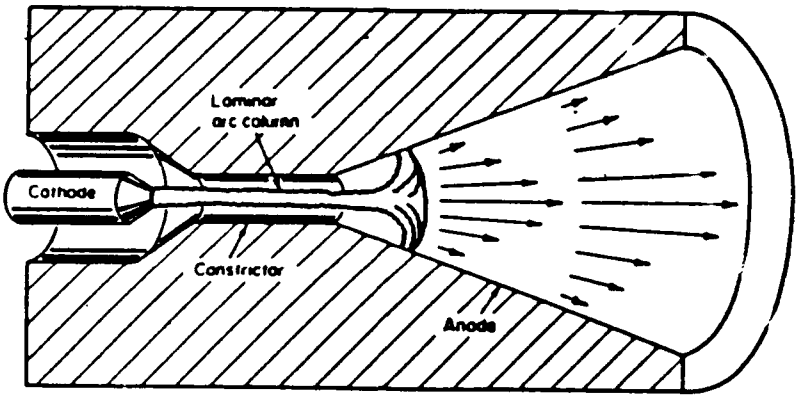

Figure 1 An Arcjet (From Jahn, Physics of Electric Propulsion)

and has led to the flight qualification of an Olin Rocket Research/Nasa Lewis Research Center (LeRC) arcjet. This thruster will be used on a General Electric satellite in the near future. It will be the first arcjet in commercial use[4].

Some fundamental questions about these thrusters remain. The quantification of heat transfer, flow conditions, arc stability, molecular make-up (i.e. percent ionized or dissociated molecules), and gas temperature profiles is ongoing or yet remains to be done. Also, no good computational fluid dynamic model exists. One essential element for determining the conditions in an arcjet and to aid in its computational modelling is to obtain static pressure measurements at various locations in

the nozzle over its full range of operation. The comparison of these profiles to cold flow (no energy added by arc) and ideal nozzle models could provide valuable insight to the operation of arcjets. The objective of this research, then, was to obtain repeatable static pressure measurements for just that purpose. Before providing details of the experiment, however, some discussion of the fundamentals of arcjet operation is in order.

1.1 Arcjet Fundamentals

As stated before, accurate analytical models for arcjets have been evasive, at best. Modelling the flow is complicated by electromagnetic and gas dynamic interactions which are still poorly understood. Temperature profiles resulting from an extremely high temperature arc extending through a cold gas, and heat transfer between the arc and the gas, the arc and the electrodes, and the electrodes (mainly the anode, which serves as the nozzle) and the gas are similarly hard to quantify. Figure 1 shows the geometric arrangement of the electrodes and the arc, the dimensions of which are usually quite small. In spite of these difficulties, the fundamental problems are not too difficult to understand.

In most modern arcjet designs, a propellant gas (usually hydrogen or a mixture of hydrogen and other gases) is channeled between two electrodes. The cathode, or negative electrode, consists of a tungsten alloy rod tapered to a point. The anode, also made of tungsten, serves a dual role as both the positive electrode and nozzle. It is usually radiation cooled, and may be oversized in laboratory models to provide more radiating area and serve as a heat sink as well.

The cathode sits in the converging section of the anode nozzle, and the spacing between the two, or the arc gap, is carefully set. The converging and diverging sections of the nozzle are connected by a cylindrical tube called the constrictor. The constrictor stabilizes the arc column and provides an area for the arc and the propellant to come into contact. Further stabilization is usually provided by injecting the propellant tangentially just upstream of the cathode tip. The resulting vortex tends to keep the hotter, lighter gases of the arc in the center of the flow while the cooler, heavier gases around the edges help keep the walls from overheating[1]. However, since the flow is extremely viscous at high temperatures, it is not clear how far downstream of the injector the swirl is a factor[5]. The vortex may have damped out entirely by the time it reaches the constrictor.

Both electrodes are constructed from tungsten, primarily because they get very hot. Anode exteriors reach temperatures of 1100 C whereas the cathode tips frequently exceed the melting point of tungsten at around 3680 K[1]. Often, the tungsten is alloyed with 2% thorium so that it emits electrons more readily. Boron nitride is used as an insulator because it also has a high melting point and is easily machinable. Where a stronger insulating material is needed, alumina is often used.

The arc itself is a core of ionized gas (from a few percent to almost fully) with temperatures ranging from 5000 to 50,000 K. Ideally, the arc attaches at the tip of the cathode (in the high pressure region of the nozzle), is carried through the constrictor as a laminar column, and attaches diffusely to the anode in the diverging section, or low pressure arc attachment region, as illustrated in Figure 1. In this region the arc attaches radially to the walls of the nozzle. Arcs are distinguished from other types of electrical discharge through gases in that they exhibit relatively low voltages (~100v), and high currents (several amps or more) between the electrodes[1].

The voltage profile between the electrodes is characterized by a sharp rise near the cathode, or cathode fall, a central region of relatively uniform voltage known as the thermal column, and another sharp rise near the

anode, or anode fall region. Net charge buildups, positive around the cathode,negative at the anode, account for the rises near the electrodes, while the central region is essentially a thermal plasma[1].

Arc formation at the cathode tip is dominated by two processes: thermionic emission and field emission. Electrons in a metal have a Maxwellian energy distribution. Those electrons which possess energy above a critical level will be emitted by the metal. That critical energy level is termed the work function, and the process is thermionic emission. It is governed by the equation

$$j = AT^2 e^{\frac{-\phi}{kT}} \qquad (4)$$

where j is the current density of emission in amps/cm^2, ϕ is the work function, k is Bolzmann's constant, and A is an empirical constant of 120 amps/cm^2-deg K^2. This is known as Richardson's equation[2]. Carrying out the calculation reveals that in order to maintain a current of several amps a cathode tip with an area considerably less than a cm^2 must be at a temperature of 2000 to 3000 K. Fortunately, this process is aided by the strong electric fields present (around 1500 V/m). Electrons in the metal which possess energy close to, but not quite equal to the work function potential "tunnel" through the potential barrier and are

emitted anyway. This combination effect is sometimes referred to as thermal field emission[6].

When an electric field is first applied to the arc gap, all stray charges in the gas drift toward the opposite electrode. Under sufficient field strengths, electrons in the flow acquire enough energy to ionize other gas molecules, creating secondary electrons. The resulting ions then impact the cathode tip with great energy, heating the cathode, which emits more electrons, and so on. This process is called Paschen breakdown, and it is an inherently unstable process. Unless it was regulated by the power supply circuitry,the current would run away, increasing until the thruster was destroyed.

The ignition method most frequently used in recent research is to send pulses of 1500-2000 V across the arc gap for a few seconds to get it started. Once the current gets moving across the gap, the voltage drops down to around 100 volts and the pulses can be disabled.

1.2 The NASA Lewis 1.2 Kilowatt Arcjet

The LeRC electric propulsion lab designed a low power hydrazine arcjet in 1986 which has been used extensively to validate the concept of using such thrusters for stationkeeping[7] (see Figure 2). Hydrazine was chosen as a

propellant because hydrazine decomposition microthrusters are the current "state of the art" in use for auxiliary propulsion for almost every satellite flying today. Since hydrazine (N_2H_4) is storable and decomposes into relatively light molecules, it is a good arcjet propellant in its own right.

For tests at LeRC, however, the use of hydrazine as a propellant is prohibited for safety reasons. A mixture of molecular hydrogen and nitrogen is used in a molar ratio of 2:1 to simulate the decomposition products of hydrazine. The only difference, then, is the temperature at which the gas enters the arcjet. When hydrazine is actually used, one expects the decomposition products to enter the arcjet at 400 - 500 C, whereas simulated decomposition gases enter at room temperature. When one compares the enthalpy of the propellant entering the thruster with the power being added to the gas, it is readily apparent that this temperature difference can be safely neglected. Experimental comparisons between the two cases show that this amounts to a 1-2% difference in thrust.

As has been previously mentioned, a number of different investigations have been done on this arcjet including a 1000 hour lifetime study[3], various nozzle designs[8,9,10], Langmuir probe analysis of the plume[11,12], and spectroscopic analysis of gas in both the plume and the nozzle[7,13]. It has

THE NASA LEWIS 1.2 KW ARCJET

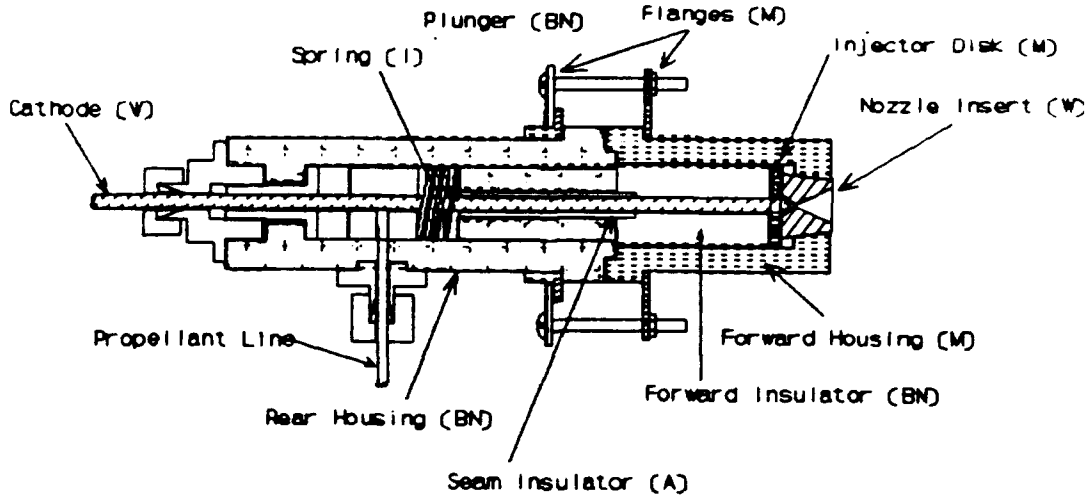

Figure 2 The NASA Lewis 1.2 kW Arcjet

demonstrated I_{sp}'s of around 460 seconds, efficiencies of 35% and a thrust level of 0.1 N. Current investigations include many spacecraft integration issues such as electromagnetic interference (EMI) and plume impingement on solar panel material, as well as the present goal, obtaining static pressure measurements along the nozzle.

1.3 Objective and Scope

The objective of this project was to obtain reliable measurements of static pressure at various points along the nozzle of a low power arcjet. These measurements were

obtained at various propellant flow rates and power settings. This provided basic information about the flow inside the arcjet which can be used both to gain understanding of observed phenomena and to verify future computer models. The measurements were taken from a thruster which was as close to the NASA Lewis 1.2 kilowatt arcjet as possible. The propellant used for all testing reported herein was a 2:1 molar mixture of hydrogen and nitrogen, or a mass ratio of 2:14.

Figure 3 shows the two types of nozzle inserts previously used at LeRC. A forward housing composed entirely of tungsten, with its nozzle machined directly into the housing, replaced the two piece design in the test article. This eliminated the concern that leaking would occur between the anode housing and the nozzle insert. The static pressure taps were then machined into the one piece housing.

Piezoresistive transducers were chosen to measure the pressure obtained from these taps. They had the required qualities of small size, high accuracy, and a fair amount of insensitivity to thermal drift.

Finally, the pressure tapped arcjet was evaluated for performance to verify its similarity to previously tested thrusters. Once thrust measurements on the tapped arcjet were made they could be used to compare with pressure profiles taken under identical operating conditions. From

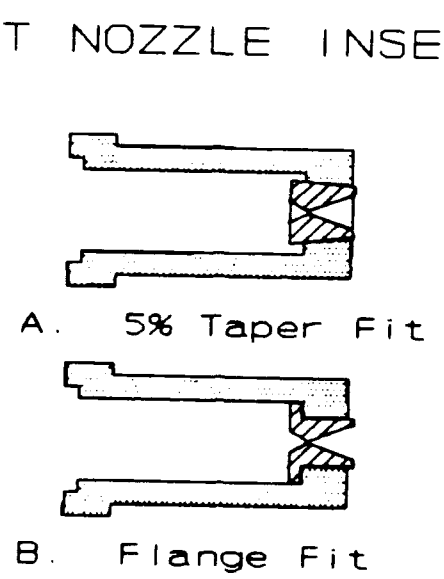

Figure 3 Types of Arcjet Nozzle Inserts

this data, specific impulse and efficiency could readily be determined, and would provide a relatively complete characterization of the thruster.

II Theory

2.1 Performance Theory

The performance parameters of electric thrusters are always important. In addition to the I_{sp} the efficiency η and the attainable thrust levels are also necessary to completely judge the utility of a given thruster.

When given as data the thrust obtained at a given mass flow is readily determined from the relationship

$$I_{sp} = \frac{F}{\dot{m} g_0} \tag{5}$$

where F is the measured thrust and m is the mass flow rate. I_{sp} data presented in Chapter 4 were calculated in this manner.

Efficiency refers specifically to power efficiency. It is usually the ratio of the thruster's jet kinetic power to the electrical power the arcjet is consuming. This neglects the energy already in the gas, however. It is more appropriate to account for the cold gas contribution to the thrust. Curran[14] did this by adding the cold flow I_{sp} to the electric power in the denominator, forming the ratio

$$\eta = \frac{W_{jethot}}{W_{arc} + W_{jetcold}} \tag{6}$$

where $W_{jet\ hot}$ is the jet kinetic power of the arcjet in operation, W_{arc} is the electrical power being used, and $W_{jet\ cold}$ is the cold flow kinetic power. Jet kinetic power for one dimensional (1D) flow is given by

$$W_{jet} = \frac{1}{2}\dot{m}(g_0 I_{sp})^2 \tag{7}$$

where m is the mass flow rate. Substituting this relationship into equation 6 and rearranging to isolate the I_{sp} terms yields

$$\eta = \frac{I_{sph}^2}{\frac{2W_{arc}}{\dot{m}g_0^2} + I_{spc}^2} \tag{8}$$

where I_{sph} is the specific impulse during arcjet operation and I_{spc} is the cold flow specific impulse. All efficiency data was calculated as in equation 8[14].

Where ambient pressure differences are present between runs, a simple correction factor can be applied to the thrust measured. This is simply the product of the exit area and the difference in ambient pressure.

Much of the data in Chapter 4 is presented in the form of nondimensionalized pressure versus specific power. Nondimensionalized pressure data is static pressure data from the throat or diverging side taps divided by the

pressure recorded simultaneously at the converging section tap.

Specific power is simply the power consumed by the arcjet divided by the mass flow rate of propellant. It has units of J/kg. Static pressure is presented herein as a function of specific power so that pressure data can be compared with performance data more readily.

2.2 Isentropic 1D Flow Theory

While there is little about arcjet operation that can be considered inviscid or isentropic, the one dimensional gas relations can be useful as a reference point. The effects of changes in the ratio of specific heats, or γ, can also be characterized by their use.

Of specific interest in this case are the ratio of static to stagnation pressure, or P/P0, and the area ratio A/A^*. The static pressure is given by the relationship

$$\frac{P}{P_0} = \left(1 + \frac{\gamma - 1}{2} M^2\right)^{-\frac{\gamma}{\gamma - 1}} \qquad (9)$$

where M is the Mach number of the flow. Assuming one dimensional, isentropic flow, the Mach number at a given point in the nozzle can be determined using

$$\frac{A}{A^*} = \frac{1}{M}\left[\frac{2}{\gamma+1}\left(1+\frac{\gamma-1}{2}M^2\right)\right]^{\frac{\gamma+1}{2(\gamma-1)}} \qquad (10)$$

where A^* is the area where M = 1. In a converging diverging nozzle exiting to a near vacuum, the sonic point is at the throat. In an arcjet nozzle, where the throat is actually a cylinder, the sonic point is assumed to lie at the junction between the constrictor and the diverging section. Previous experiments[15] have shown this to be true for an operating arcjet, while the sonic line lies at the constrictor entrance during cold flow.

One dimensional nozzle theory, however, tells nothing about static pressure behavior during arcjet operation. One approach to this problem would be one dimensional flow with simple stagnation temperature change, or Raleigh flow. As above, this approach assumes constant γ and inlet conditions. It predicts that as the temperature increases the flow will thermally choke, lowering the mass flow which the nozzle can permit[16]. In this case, however, the mass flow controllers increase the inlet pressure in order to maintain a constant mass flow rate through the throat. Also, the vast temperature changes in the propellant gas during operation would similarly invalidate the constant γ assumption.

Other one dimensional assumptions, however, can give a coarse accounting of the process. The perfect gas equation

of state can be modified to account for the change of the total number of moles present, giving

$$P = Z\rho RT \tag{11}$$

where R is the propellant gas constant, ρ is the density, and T is the temperature. The compressibility factor Z is defined as the ratio of the number of moles in a system resulting from dissociation in a heated state divided by the number of moles originally present in some cold state[17]. Forming a ratio between conditions at a heated state and a cold one yields

$$\frac{P_2}{P_1} = \frac{Z_2\rho_2 T_2}{Z_1\rho_1 T_1} \tag{12}$$

where subscript 2 refers to the heated condition while 1 refers to cold gas flow. Change in R between state 1 and state 2 due to dissociation is accounted for by the ratio Z_2/Z_1. From continuity the relationship $\rho_1 u_1 = \rho_2 u_2$ can be used to eliminate density from the equation. Also, Z_1 is unity by definition.

This leaves three factors which must be estimated. From performance data, the ratio u_2/u_1 can be determined at the exit of the nozzle. This ratio is assumed to be constant throughout the nozzle. What remains is the estimation of the compressibility factor Z_2 and the temperature ratio.

2.3 Temperature Estimation

When the gas temperature reaches temperatures in excess of 3000 K, the specific heat at constant pressure C_p can no longer be assumed to be constant. One must appeal to physical gas dynamics to determine the enthalpy of the gas at a given temperature. If the dissociation of the gas is known, the specific enthalpy of the gas can be predicted with great accuracy. Unfortunately, the level of dissociation is also a function of pressure, which complicates the situation to the point where one must rely on experimental data or numerical simulations of conditions in the flow. The first is not generally available for arcjets, while the second is beyond the scope of this research.

Asymptotic behavior at temperature extremes can be modelled quite well, however. Below 2000 K, the gas is composed completely of molecular hydrogen and nitrogen and thus follows the enthalpy curve for that mixture. Hydrogen dissociation at one atmosphere begins around 2500 K and is relatively complete at a temperature of 5500 K[1]. Nitrogen begins dissociation around 4000 K and is relatively complete around 9000 K[18]. Using composition curves from references 1 and 17, a graphical estimation of the temperature-enthalpy diagram for the mixture can be made.

To make this estimation one must first compute the asymptotic curves. The enthalpy for molecular hydrogen, ignoring dissociation and ionization, is given by

$$h_{H_2} = \frac{7}{2}RT + \frac{1.5R\theta_{vib}}{e^{\frac{\theta_{vib}}{T}} - 1} \qquad (13)$$

where θ_{vib} is the characteristic vibration temperature, which for hydrogen is 5980 K. For molecular nitrogen, the relationship is quite similar:

$$h_{N_2} = \frac{7}{2}RT + \frac{\theta_{vib}R}{e^{\frac{\theta_{vib}}{T}} - 1} \qquad (14)$$

The characteristic vibration temperature for molecular nitrogen is 3390 K^2. The simulated hydrazine decomposition mixture contains hydrogen and nitrogen in a mass ratio of 2:14. Using this, asymptotic enthalpy for the mixture at temperatures up to 2500 K can be determined.

The enthalpy of the completely dissociated mixture is calculated in a similar fashion. Here, gases are treated as monatomic, having only translational components to their enthalpy. A large amount of energy has gone into the formation of H and N, and this is accounted for by including the specific heats of formation, Δh_f°. For both atomic nitrogen and hydrogen this is given by[2]

$$h = \frac{5}{2}RT + \Delta h_f^\circ \qquad (15)$$

The specific heats of formation for atomic hydrogen and nitrogen are 21.79 x 10^7 J/kg and 3.376 x 10^7 J/kg respectively.

Once one has a chart containing these two asymptotes for the mixture, a curve can be sketched in to estimate the behavior in the temperature region where dissociation has begun but is not complete. Individual dissociation curves from references 1 and 18 were first sketched between the asymptotes and a composite curve was drawn by adding these two (see Figure 4).

The resulting curve was then linearized for a region between 3500 and 4400 K, corresponding to specific enthalpies between 15 and 30 MJ/kg. The slope in this region, or the average C_p, was estimated at 16,667 J/kg-degrees K.

The compressibility factor was estimated similarly. From the charts in references 1 and 18 at one atmosphere, at 3500 K hydrogen was assumed to be 30 percent dissociated while nitrogen was 0% dissociated. At 4400 K, these figures were 90% and 10%, respectively. This yielded a compressibility factor of 1.2 at 3500 K and 1.63 at 4400 K. A linear interpolation between these two extremes was used to estimate Z in the region.

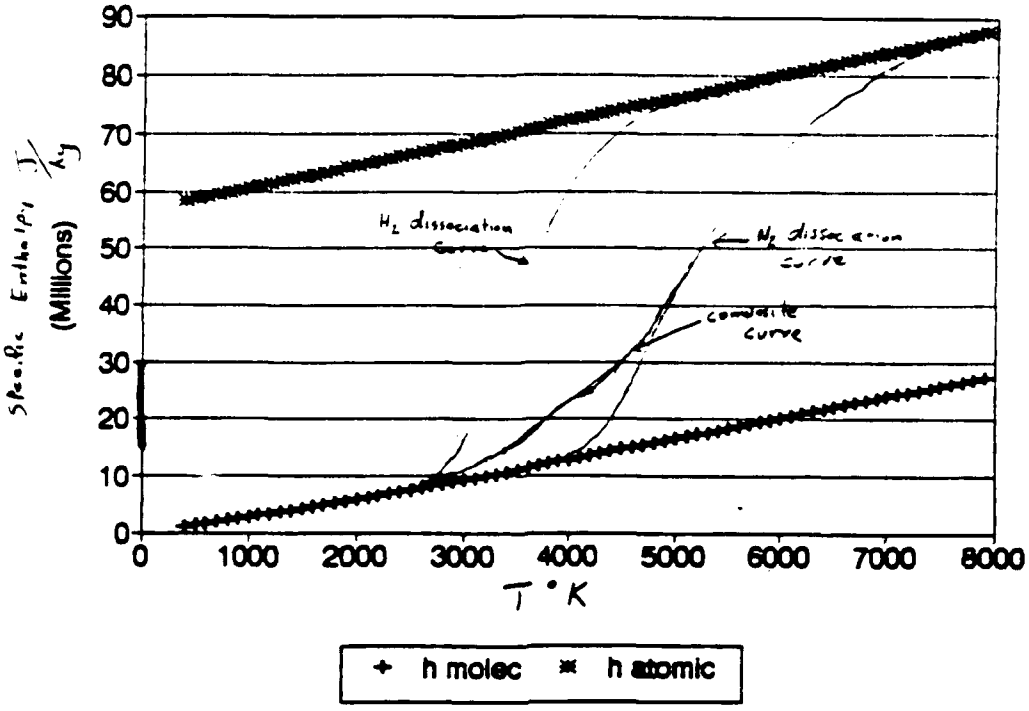

Figure 4 Estimated Temperature Enthalpy Diagram for Hydrazine Decomposition Products

This graphical technique yields an estimate for the stagnation temperature rise for a given heat added. However, the simple thermodynamic model used in the previous section uses the ratio of static temperatures between a hot and cold flow. In a real gas, the static temperature ratio will not be equal to the stagnation temperature ratio at a given tap location. For this model, however, the two ratios will be assumed to be equal and independent of nozzle area ratio. This allows the substitution of stagnation temperature ratios in equation 12 rather than static

temperature ratios. Comparisons of this model with experimental data are given in Chapter 4.

2.4 Arc Stability

An arcjet is said to be stable when it operates consistently at a steady voltage and in "high mode." High mode refers to a diffuse arc attachment in the low pressure (diverging) section of the nozzle. Conversely, "low mode" is the case where arc attachment to the anode is in the converging section, nearest the cathode. Since the arc voltage is roughly proportional to the length of the arc, "high" and "low" refer to the arc voltages characteristic of each.

Unstable arcjet operation was observed to be accompanied by a fall in average arc voltage, while the voltage itself fluctuated as much as 30 or 40 volts. During this time, the arc was thought to be transitioning between high and low mode operation, failing to seat permanently in either position. Transition between stable and unstable behavior was sudden and unpredictable.

Two factors which influence stability are arc current and propellant flow rate. The higher either is, the more stable the arc will run. Higher flow rate is the stronger of the two trends, and it stabilizes the arc because it

increases the strength of the vortex and because it tends to blow the arc downstream, toward the diverging section. It is unclear why arcs with higher current run more stable. See Appendix C for stripchart records which demonstrate unstable behavior and trends.

III Experimental Setup

The experimental work for this research was conducted entirely at the NASA Lewis Advanced Propulsion Division Electric Propulsion Lab (Bldg 301), which sponsored the research. All of the following equipment was drawn from resources available there, with the exception of instrumentation specifically for obtaining pressure measurements, which were ordered directly. It is important to keep in mind that all equipment at NASA Lewis Research Center (LeRC) is calibrated and otherwise evaluated for accuracy on a regular basis, including stripchart recorders, multimeters, and oscilloscopes. This was done in addition to other calibration techniques specifically mentioned. The expected accuracies of the equipment are discussed below.

3.1 The Pressure-tapped Arcjet

As mentioned above, the only major difference between the thrusters previously used at LeRC and the test article for pressure measurements was the forward housing. For more information on the NASA LeRC standard design, see Appendix A. Concern over leakage led to the use of a one piece design where the nozzle was machined directly into the 2% thoriated tungsten forward housing. This nozzle is

similar to those used in previous research, consisting of a 30° converging section half angle, a constrictor 0.010 inches in length and 0.025 inches in diameter, and a diverging conical half angle of 20°. The area ratio of the nozzle, or ratio of the exit area divided by throat area, is 225. The complete specifications for this housing are given in Table 1 and Figures 5 & 6.

Complete details of the modifications necessary to obtain static pressure measurements on the arcjet, as well as methods used to determine the exact location of the taps after modification, are given in Appendix B. The axial

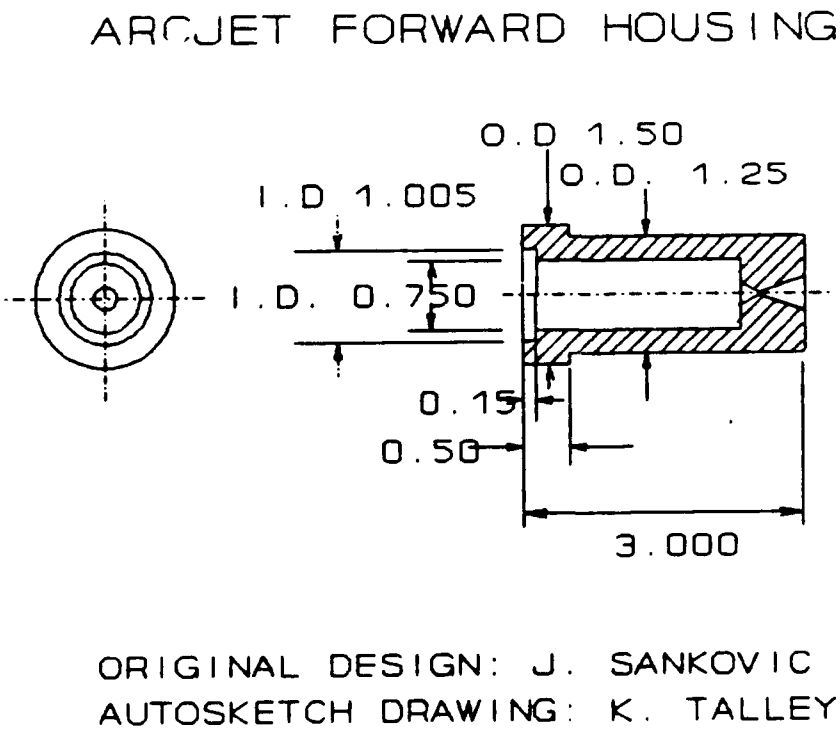

Figure 5 One-piece Forward Housing Design

NOZZLE CONFIGURATION

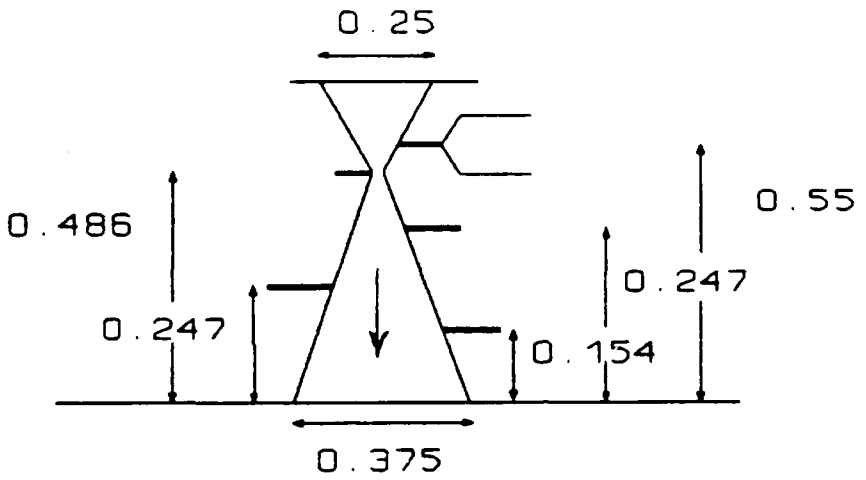

Figure 6 Layout of Tap Locations

Table 1 Forward Housing Specifications

LENGTH	3.00 in	LIP DIAMETER	1.50 in
INNER DIAMETER	0.750 in	OUTER DIAMETER	1.25 in
INLET DIAMETER	0.250 in	EXIT DIAMETER	0.375 in
CONVERGING 1/2 ANGLE	30 deg	DIVERGING 1/2 ANGLE	20 deg
CONSTRICTOR LENGTH	0.010 in	CONSTRICTOR DIAMETER	0.025 in
MATERIAL	2% THORIATED TUNGSTEN		

locations of the taps, their designations, and other pertinent information about the five taps is given in Table 2. The assembled arcjet is depicted in Figure 7.

NAME	DISTANCE FROM EXIT	AREA RATIO	ISENTROPIC P/P0
FEED	EXTERNAL	_____	1
CONVERG TAP	0.55 in	13.9	0.9994
THROAT TAP	0.486 in	1	0.5283
1/4 TAP	0.370 in	17.86	3.092×10^{-3}
1/2 TAP	0.247 in	60.96	5.20×10^{-4}
3/4 TAP	0.154 in	110.6	2.22×10^{-4}

Table 2 Tap Summary

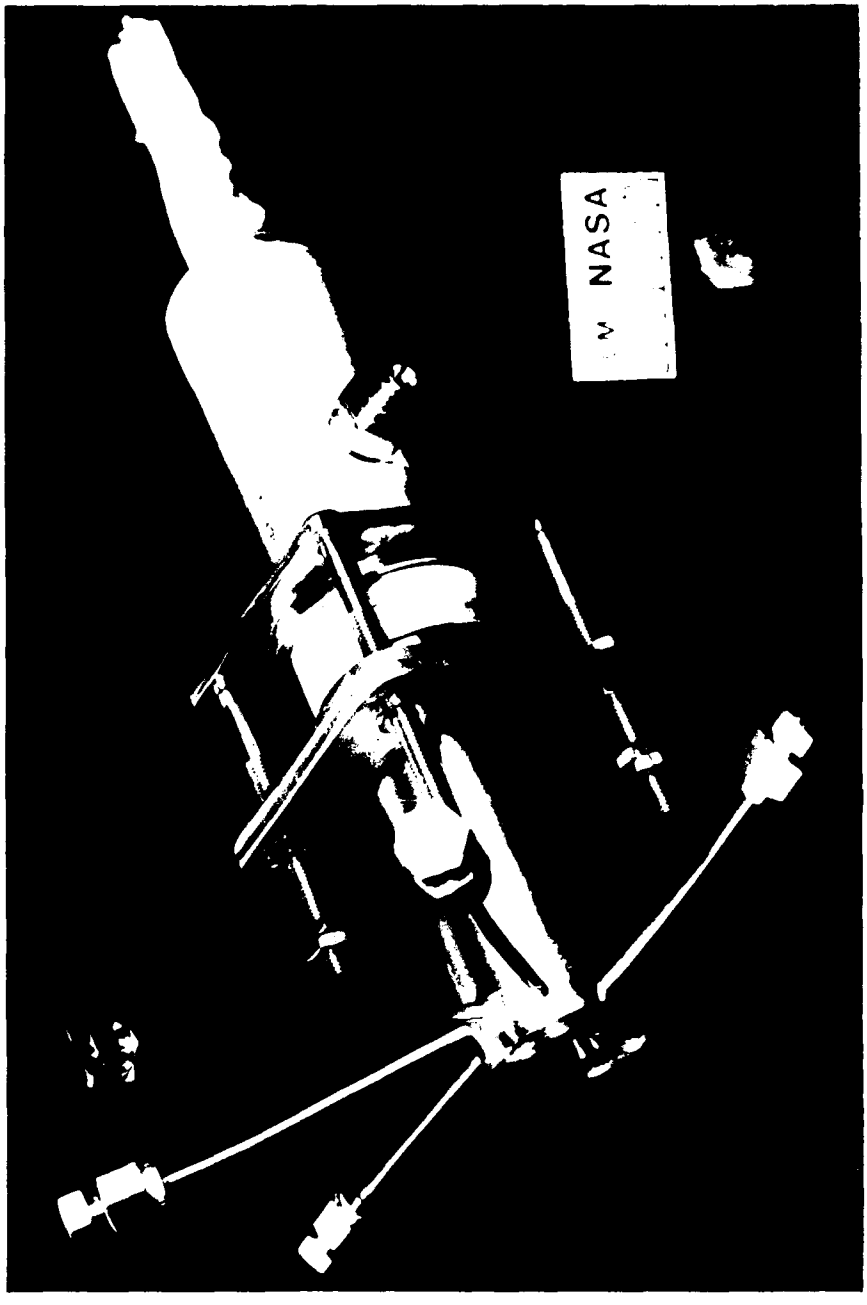

Figure 7 Pressure Tapped Arcjet

3.2 Pressure Measurement Apparatus

To simplify the design, all pressure measuring equipment was designed to fit inside Bell Jar 7 (see Section 3.3). This eliminated the necessity of running five tubes out of the vacuum chamber through feed throughs and the inevitable complications this would have caused.

Each of the five molybdenum tubes projecting from the assembled test article was fitted with a 1/8 inch stainless steel Swagelok fitting. To these were attached either a cap, for times when a particular tap (or all of them) were not needed, or another fitting joining the tap to the transducer block. This link consisted of a 1/8 inch stainless steel tube between 13 and 18 inches long. This led from the anode of the thruster upward towards the transducer block, which was mounted beneath the lid of the bell jar. Since these tubes were not insulated from the anode, and indeed would conduct both electric potential and heat, the anode and as a result the pressure links as well, were grounded. This prevented any arcing to the sides of the bell jar, which for some links came within an inch of the apparatus when the lid was lowered. To provide electrical isolation from the arcjet, as well as a "fuse" in the system should the links get too hot, the final four

inches of the links were a 1/8 inch plastic tubing. The tubing was flexible and thus made installation and removal of the arcjet much easier than would have been possible with stiff fittings.

The transducer block itself was simply a rectangular box of aluminum, with 1/8 inch pipe fittings for the plastic tubing machined in one side and 10-32 x 0.30 inch threads in the other for mounting the transducers. Teflon tape was wrapped around the pipe fittings to achieve a good seal, while the transducers were sealed with the O-rings with which they come equipped (see Figure 8).

Only four transducers were available for simultaneous use, and one of the pressure taps was capped at the thruster at all times. Each transducer, when properly connected to an appropriate tap, constituted a channel, which were labelled I-IV. For a summary of the channel configurations, see Table 3. Endevco piezoresistive transducers were selected for this experiment. Determination of measurement ranges for each channel was based on a one dimensional analysis of cold gas flowing through a DeLaval nozzle of identical geometry. Chamber pressure for this was assumed to be 50 psi, and the resulting static pressures at various points in the nozzle were calculated using a ratio of specific heats of 1.4. This particular γ is appropriate for a room temperature mixture of diatomic gases. Each channel

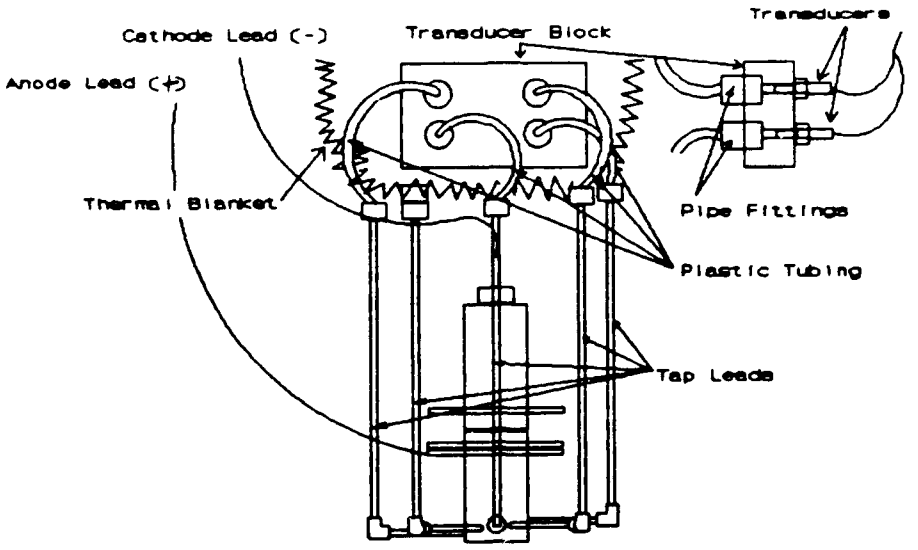

Figure 8 Setup Inside Bell Jar

Table 3 Channel Configurations

	CHANNEL A	CHANNEL B
CONVERG TAP	X	X
THROAT TAP	X	X
1/4 TAP	X	X
1/2 TAP		X
3/4 TAP	X	

was given the smallest range possible to achieve better resolution and accuracy. The transducers used in this research measure pressure by means of quartz strain gauge elements, which are very small solid state silicon resistors arranged in a four arm Wheatstone bridge. The strain gauge elements are incorporated into a diaphragm which is very sensitive to pressure differences across it and is flexed accordingly. The strain gauges change resistance according the amount of flexure of the diaphragm, producing a voltage on the output arms of the bridge proportional to the pressure difference across the diaphragm[19]. When one side of the diaphragm contains a reference vacuum, the pressure is measured with respect to zero and is referred to as an absolute pressure. On some transducers, the reference side of the diaphragm is vented to the external environment, the pressure is measured with respect to that and is termed a relative pressure. When this relative pressure is standard atmospheric, then measurement is known as gauge pressure. For channel IV, which was invariably connected to the converging section tap, the Endevco 8530C-100 was chosen. Its range was from 0-100 psi absolute (psia). Like all of the transducers used, it internally compensated for temperature up to a rated maximum temperature of 200°F. At that temperature, it showed a sensitivity shift of 0.44% of full scale output (%FSO), a zero shift of 0.87% FSO, and

non-linearity and hysteresis of less than 0.1% FSO each. Simply put, if the transducer was at a temperature of 200°F and exposed to a pressure of 100 psi, the combined effects of sensitivity shift and zero shift would mean the pressure signal output would be 101.3 psia. When returned to a vacuum the zero would have shifted so that the pressure would then read 0.9 psia rather than 0.0. These factors were included in the error analysis and are reflected in the error bars on experimental data.

Channel III, which was always connected to the throat tap, was instrumented with an Endevco 8530C-50, which had a range of 0-50 psia. During initial calibration at 200°F, it was determined to have a sensitivity shift of -0.31% FSO, a zero shift of -0.68% FSO, and non-linearity and hysteresis of less that 0.1% each.

Relative pressure gauges, namely two Endevco 8510B-2's, were used to measure static pressures in the diverging section of the nozzle. During operation, the output pressure of each was referenced to the pressure in the bell jar. The transducers had a range of ±2 psi relative, which was chosen to better measure the lower pressures expected in this section. The two transducers were numbered 1 and 2 upon receipt to prevent confusion, and were placed in channels I and II, respectively. During initial calibration at 202°F transducer #1 demonstrated a sensitivity shift of

2.07% FSO, a zero shift of -0.66% FSO, a non-linearity of 0.27%, and a hysteresis of 0.1%. For #2 under the same conditions the sensitivity shift was 1.3% FSO, the zero shift was -.93% FSO, the non-linearity was 0.24%, and the hysteresis was less than 0.1%.

The calibrations done above were performed upon delivery from the manufacturer by Cortez III Service Corporation. They represent the "worst case" deviations from an ideal, perfectly linear instrument. The sensitivities for each transducer, i.e. how many volts/psi, were also determined. Unfortunately, these represent the only end to end calibration of this equipment performed during the experiment, as periodic in situ calibration proved to be impractical. The sensitivities for each were entered into the display unit for each channel.

The output for each transducer was fed through a Deutch connector to the exterior of the bell jar, where they were connected to four Endevco Model 4428 piezoresistive pressure transducer minisystems. Each 4428 provided voltage excitation to the transducer, signal conditioning, and a digital readout in psi or millivolts. Additionally, these units provided a ±5 volt buffered output which was used for oscilloscope traces and automated data acquisition. The frequency response of this output was rated from dc to 30 kHz.

The four minisystems were individually adjusted for the particular transducer they were wired to in two ways. First, the range of the transducer to be condition was chosen by means of a selector on the rear of the unit. Secondly, the sensitivity was entered for each unit based on the calibration value. This ensured that the correct pressure was displayed by each unit.

The Model 4428 was rated with gain errors of less than ±0.5% FSO, a thermal gain shift of ±0.2% FSO at 131°F, and a gain zero stability of ±2.8 microvolts/°F. The units were evaluated upon delivery and met these specifications.

Each unit had a display of four digits. The resolution of the units set to the ±2, 50, and 100 psi ranges was then 0.001,0.01, and 0.1 psi respectively.

3.3 Vacuum Facilities

The majority of the testing was done in Bell Jar 7 (see Figure 11). The facility was 0.64 m in length and 0.64 m in diameter, in which the arcjet was mounted vertically from the bell jar's lid. Vacuum was maintained by a single mechanical roughing pump with a 21,000 liter/minute capacity, which also serviced another, identical bell jar. When propellant was running in both jars, the background pressure in Bell Jar 7 could go as high as 1.36 torr (0.026

psi) but were usually between 0.8 and 0.9 torr (0.015 and 0.017 psi) when propellant was running in Bell Jar 7 alone. Identical test runs were made at each extreme with excellent agreement between the results.

The vertical mount in the bell jar did not contain a load cell, so performance testing was done in Tank 8, which was 1.5 m in diameter and 5 m long. Vacuum was provided by four 30,000 liter/minute oil diffusion pumps backed by a rotary blower and a mechanical roughing pump. Access to the vacuum was provided by a 0.9 m diameter by 0.9 m long port extension in which the arcjet and thrust stand were located. The extension was located at one end of the tank and separated from it by a 0.9 m gate valve[11]. While testing at lower flow rates, the background pressure in the tank was maintained below 5×10^{-4} torr. When testing at higher flow rates, there was concern that the ambient pressure would exceed the rating of the diffusion pumps; therefore, they were shut off. For these runs, the blower and roughing pump were left on, resulting in an ambient pressure of around 0.25 torr (5×10^{-3} psi). The diffusion pumps were not always on when it was possible to use them, as the startup and shutdown cycle for them was three hours each. Time constraints made frequent switching of the two operating modes impossible.

3.4 Thrust Measurements

During testing in Tank 8 the arcjet was mounted horizontally on a thrust stand (see Figure 12). The stand was composed of a moving fixture upon which the thruster rested which was itself mounted by flexures to an immobile platform. The displacement of the stand relative to the platform was measured by a linear variance displacement transducer, or LVDT. To assure that the relationship between thrust applied and displacement was as linear as possible, all wiring, propellant and water cooling lines were coiled perpendicular to the thrust axis. Since the stand was designed to minimize friction, the stand was actively magnetically damped along the direction of the thrust axis. To minimize thermal drift, all electronics in the thrust stand were shielded by a water cooled copper sheath. The support column beneath the moving fixture was also water cooled.

The restoring force on the moving fixture was a result of the combined effects of the flexures, coiled wiring and water cooling tubes, and gravity. Therefore, the test stand was calibrated by a series of 4 gram weights hung from the moving fixture by a windlass and pulley. This was done in place and under vacuum immediately prior to the start of each test. Two measurements at each weight were taken and

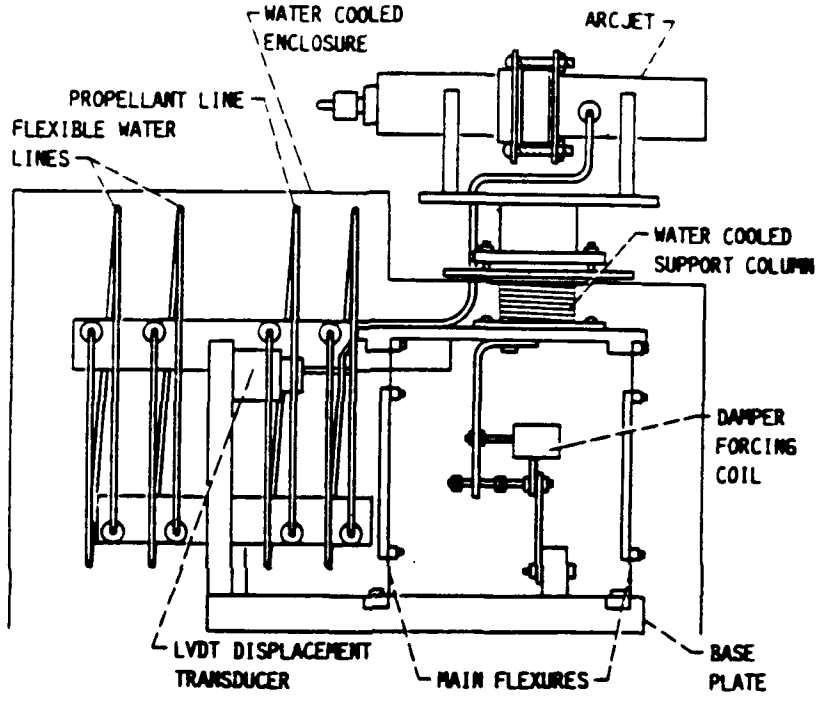

Figure 9 Tank 8 Thrust Stand (from ref. 13)

averaged, and were repeatable to within less than 1 percent[4]. During thrust testing a tare weight of 4 g was maintained on the thrust stand, chiefly to maintain tension on the windlass and keep the monofilament holding the weights slung correctly.

3.5 Propellant Supply

As previously mentioned, the propellants used were gaseous mixtures of room temperature hydrogen and nitrogen. In some cases, however, pure hydrogen was also run, but under a very narrow operational envelope. This was primarily due to the mass flow limitations of the available mass flow controllers (see below).

The gases used were UHP (ultra-high purity) grade. The hydrogen was of a purity of greater than 99.9995 percent, contained less than 1 part per million (ppm) oxygen and less than 1 ppm water, while the nitrogen had a purity of greater than 99.999 percent, with less than 1 ppm oxygen and 3 ppm water. The two propellants were stored separately and fed to the flow controllers at a pressure of around 150 psi[5].

The mass flow controllers used were Unit Instruments mass flow controllers with an output of 10 standard liters per minute (SLPM). These were used for both gases in both Bell Jar 7 and Tank 8. They were rated with an accuracy of ±1% of full scale, with non-linearity and repeatability of the indicated flow rated at less than 1%. These parameters were confirmed by calibration of the flow controllers in both facilities.

The flow controllers were individually calibrated by diverting their output from the vacuum chamber to an instrumented calibration tank the volume of which had been carefully determined previously. The valves which diverted the gas were switched electronically by a control circuit and gas was allowed to flow into the calibration tank for two minutes. The exact period that the valve was open was displayed with a resolution of a tenth of a second. Using temperature and pressure measurements from the tank from both before and after the gas entered, the number of moles of gas in the tank could be calculated. By dividing the number of moles which flowed in by the flow period, and multiplying by the gas's molecular weight, the mass flow of the controller could be determined accurately. This is done for both hydrogen and nitrogen separately and for several points from zero to full scale.

Mass flow calibration for Bell Jar 7 was done by means of a portable cart which contains all of the necessary valves and control circuitry. At Tank 8, however, this apparatus is permanently installed for ease of use.

The flow controllers were operated by a master control unit from which it was possible both to set and monitor the flow settings. These control units were rack mounted and readily accessible.

Any time gaseous hydrogen is used, careful attention must be given to safety. In this case several measures were taken to ensure that hydrogen never mixed with the air in the laboratory. The control panels for both vacuum facilities ensured that the flow controllers for all gases were only powered when the vacuum chambers were closed and connected to an operating vacuum pump. Furthermore, all lines containing hydrogen were alternately purged with nitrogen and pumped to vacuum several times before being disconnected or reconfigured. All propellant plumbing work outside of the vacuum chamber itself was done only by qualified operators. The output from the vacuum pumps was mixed with ballast nitrogen before being vented to the atmosphere outside the building. As an additional precaution, all areas where hydrogen was used were clearly marked and equipped with hydrogen and low oxygen alarms.

3.6 Power Supply

Arcjet power supplies must provide for efficient, stable operation of the thruster as well as a reliable and nondestructive starting circuit. This is complicated by the fact that arcs do not possess a typical resistive voltage-

current characteristic, i.e. where the voltage drop across the circuit increases with current, as in a resistor. Rather, the mechanics of charge carrier formation in the arc give it what is known as a negative resistance slope, where the opposite is the case. A further complication to the design of a power supply is that it must emulate the flight hardware for which it is acting as a laboratory model, so that the thrusters and the power supplies can evolve simultaneously toward flight qualified hardware. This means that power transformation must be DC-DC, with the resulting ripples in the power signal this produces[11].

The portable power supply used for this experiment, the "Arc Jet Driver Mark VI," met all of these requirements. The control circuitry provided current controlled, stable operation for the thruster. Arc ignition was accomplished by a series of high voltage pulses provided by the interrupted charging of a large inductor. This quickly started the arcjet under most circumstances. The desired arc current, magnitude of the starting pulse, and period of the pulses could be set by potentiometers to the desired values. Throughout the testing, the pulse voltage was limited to around 2000 v (although arc breakdown occurred before it reached this limit in most cases) and fired about

four times per second. Under most circumstances the arc was started at about 11 amps. As the supply was portable it was used in all experiments except for one, where a minor repair forced the use of its predecessor the Mark V while repairs were made.

The Mark VI was nominally rated at 1.2 kW, although it exceeded this occasionally with no degradation in performance. It could sustain up to 18 amps but never exceeded 16 A during testing.

One problem experienced with this power supply was EMI. The starting pulses generated an incredible surge of interference to the point where the operation of some nearby electronics was impaired. Although instrument cables were reasonably well shielded, erroneous data was generated during the operation of the starting circuit. Fortunately, startup was limited to a few seconds only, and this did not result in the loss of any data not specifically taken during that time, however, the problem was discovered too late to develop any workarounds.

3.7 Power Measurement

Voltage and current characteristics were recorded for the arcjet during all experiment runs. The voltage was recorded in two ways, depending upon the instrument for which it was needed. The primary method was the measurement of the voltage between the anode and cathode leads by an isolated Fluke 8050A multimeter with a rated accuracy of ±1% of the indicated reading. For this measurement it was set to record DC voltage at a range of 10V-200V with a resolution of 0.01V. For stripchart and automated data acquisition a 100:1 isolated voltage divider was used. It was placed between the power supply and the arcjet leads. No calibration data was available for this amplifier, but voltages measured from it usually agreed with multimeter readings to within 5%.

Current was measured two ways. For automated data acquisition the voltage drop across a current shunt located inside the voltage divider mentioned above. Again, specific calibration information was not available for this device, but the signal generated by this method was within a few volts of that measured with the multimeters. However, the data generated thus was used for qualitative analysis only.

The majority of current measurements made for this experiment were made by a Hall effect current probe, the Tektronix P6303. This probe was calibrated daily by means of a DC current loop attached to a separate power supply. The probe was calibrated at the intended operating currents for that particular day (usually integer values), with additional calibration points taken on the high and low end. Each point was recorded twice and averaged. Once calibrated this way, the current probe was accurate to ±0.1 amp[3]. This calibration was further confirmed by the fact that potentiometer settings on the power supply consistently produced the same indicated arc currents at a given flow rate.

The current meter was supported by a Tektronix AM 503 Current Probe Amplifier. The output from this amplifier was routed to a second Fluke 8050A multimeter, also isolated.

3.8 Data Recording

For the most part, data was recorded by hand into a research notebook at five minute intervals. However, certain data points were recorded permanently by a Linseis

2025 two channel chart recorder. This chart recorder and associated amplifiers were rated at an accuracy of 0.25% with non-linearity and hysteresis of less than 0.15% each. The chart recorder met or exceeded these standards at its last calibration in June of 1990.

The stripchart usually recorded one channel of pressure data from the buffered output of the pressure minisystems and one channel of voltage data taken form the isolation amplifier. This data was used mostly to analyze arc stability and the interrelation of arc voltage, pressure, and stability. The data was typically recorded at a rate of 10 cm/hour.

3.9 Experimental Procedure

The main goal of this research was to obtain pressure profiles along the nozzle of an arcjet across the entire operational envelope of the thruster. Also, the performance of the thruster was characterized and correlated with the pressure data.

After initial assembly of the experimental apparatus the arcjet was run at 10 A for 20 hours to "burn in" the

cathode. Burn in was the period during which the arc makes a small crater on the tip of the cathode, in which it normally attaches. During this time the thruster was observed to be running extremely unstable. When it became clear that the instability was not lessening during burn in, the thruster was removed and disassembled for inspection. It was discovered that the Grafoil gasket separating the injector and the front housing had slipped out of place (see Appendix A), allowing propellant flow to bypass the injector disk and creating an asymmetry in the flow entering the constrictor. Either of these factors, asymmetry or non-vortical flow, could account for extremely unstable operation. This problem was corrected and the thruster reassembled. Following this, the arcjet ran significantly more stable, but the instability problem did not disappear. All data reported herein were taken after this time.

The typical mass throughput of LeRC 1.2 kilowatt arcjet is 35 to 50 mg/sec of simulated hydrazine decomposition gases. To improve stability, this nominal range was extended to 65 mg/sec. Thus, the arcjet was run at three different mass flow rates: 35, 50 and 65 mg/sec. For each flow rate data was obtained at various current levels, with the lower boundary set by the total absence of a stable

operating point while the upper boundary was set at either 14 A or a specific power in excess of 30 MJ/kg.

When possible, all data for a given flow rate were taken during the course of a single run. The in-place calibrations previously described were performed immediately prior to data collection. At the start of each run, the thruster was allowed to warm up for a period of thirty minutes to one hour, usually at a current of 11 A. Following this, the current was stepped through the entire envelope, staying at each point for thirty minutes. This was to allow the arcjet to settle into each operating point. Finally, the arcjet was returned to its initial amperage to ensure repeatability. For the same reason, some runs were repeated several times.

Data was taken at all flow rates and amperages for each of the two pressure channel configurations listed in Table 3. Since three of the four channels measured the same tap in each case, this also added to repeatability.

Following the collection of pressure tap data in the bell jar, the pressure taps were capped and the arcjet was mounted in Tank 8 for performance testing. The same procedure was used, and the currents were varied in the same order. Background pressure was the only major difference

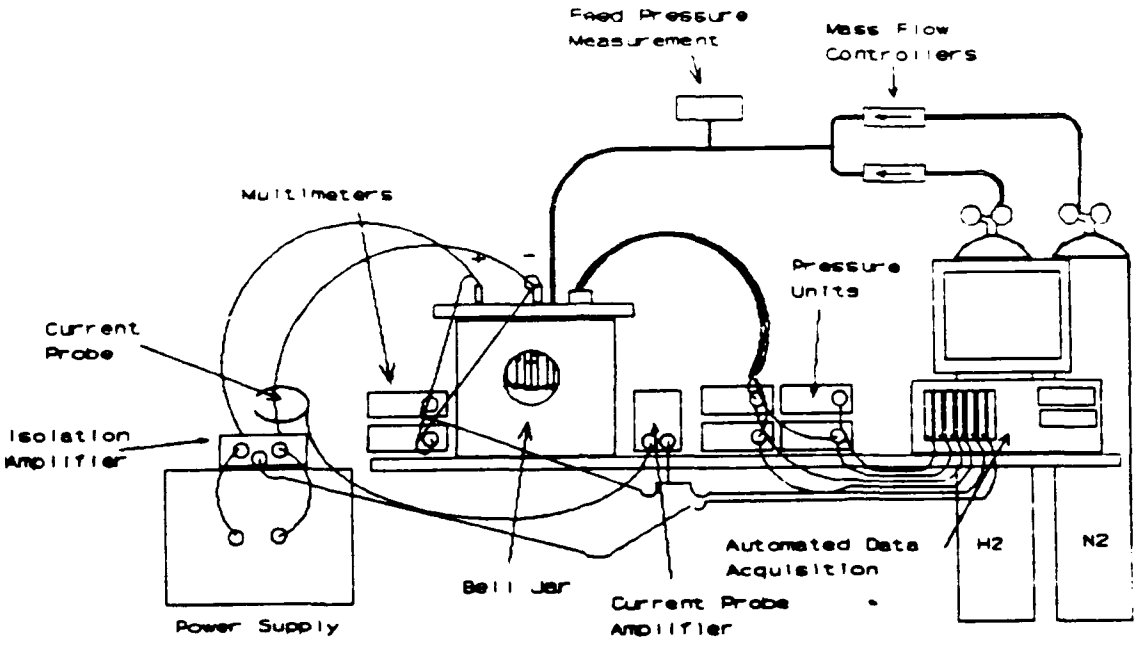

Figure 10 Schematic of Bell Jar 7 Setup

between the two vacuum chambers. This difference was corrected for, as one expects the thrust from such a device to be sensitive to this (see Section 2.1).

During testing, the thruster was periodically removed so that the nozzle, cathode and throat could be examined by a fiber optic boroscope. Video tape recordings were made of these examinations. Additional video recordings were made of the thruster while operating in Tank 8.

IV Results and Discussion

4.1 Synopsis of Results

As has been previously mentioned, arc stability was a major factor in the data collection. Since most of the data were taken by hand, the rapid fluctuations caused by instabilities made data collection impossible during those intervals. However, during stable operation the data were steady and easily recorded. All data presented herein were taken during stable, steady state operation unless otherwise stated. Appendix C contains stripchart records which demonstrate both stable and unstable behavior.

Steady state in this context means that the arcjet had been given time to reach its operating temperature. Thermal equilibrium is desirable because the walls of the anode contribute a significant amount of the heat transferred to the gas. After a step change from one current level to the next, the measured performance from previous arcjet research took ten to fifteen minutes to settle into steady state operation. By waiting thirty minutes before taking data, repeatable performance data is assured. The arcjet for this research conformed to that standard for performance data,

but measured static pressure was another case. The pressure data taken at the end of the run was consistently higher by five to ten percent than that taken after warmup at the beginning of the run. Increasing the initial warmup period to one hour produced no improvement.

The exact reason for this was unknown. The change in the forward housing design from a two piece construction with a tungsten nozzle insert to a solid tungsten forward housing may have had a role in this. During operation with the standard design, the nozzle insert was visually observed to be quite a bit hotter than the molybdenum housing, despite the fact that the two are in excellent contact. In this case, however, there was only one piece which was considerably larger than the nozzle inserts used in previous research. This could account for the longer settling time required. Pressure data from the 1/4 tap was plotted versus time in Figure 11. Step changes visible on the figure represented progression through the operational range of arc current in intervals of one Amp. The mild positive slope of the data between these changes was caused by thruster warming. Data samples significantly above the rest for a particular time were sampled during periods of instability.

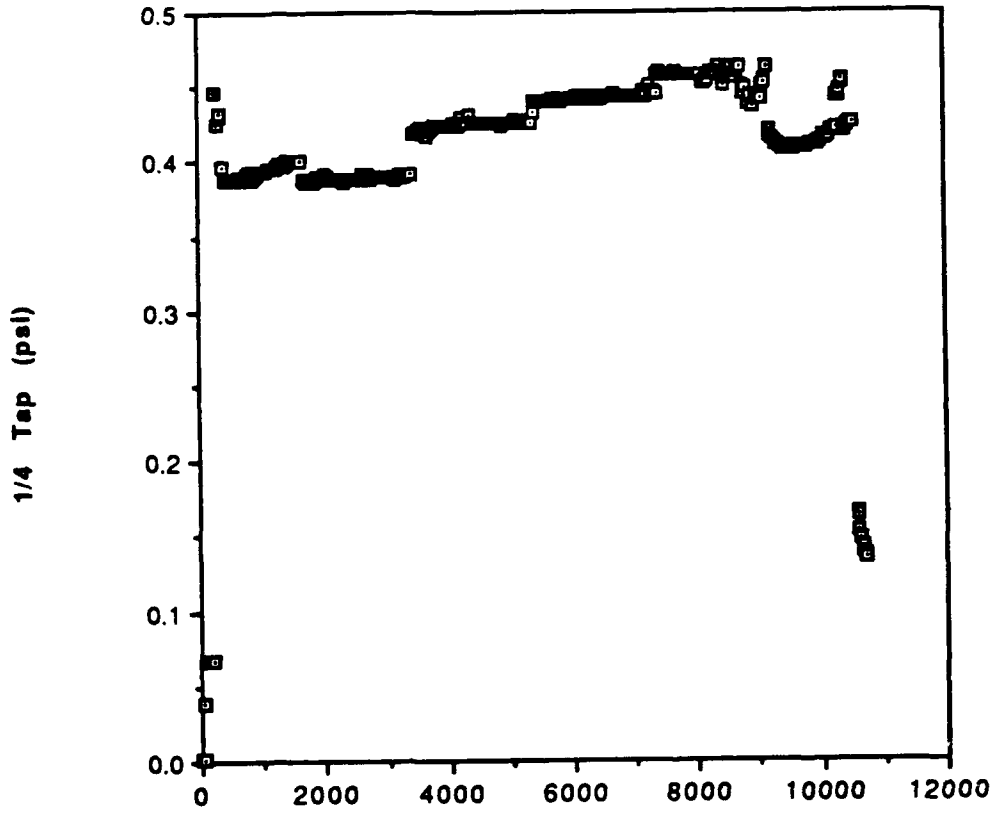

Figure 11 Static Pressure vs Time for a Typical Data Run (50 mg/sec)

However, the data collected during this research showed good repeatability, usually within five percent. The static pressure rose linearly with power in all cases. This was partially due to the mass flow controllers' maintenance of a constant flow rate. As the average temperature of the gas in the nozzle throat rose during arcjet operation, the flow

controllers increased the back pressure to compensate for lowering density. By nondimensionalizing the pressure data with the converging tap pressure, this effect has been accounted for. Behavior of pressure ratios was due to phenomena in the arcjet, not the propellant feed mechanism.

The pressure ratios in the diverging section showed a mild linear rise with increasing specific power. This was consistent with previous research done on a 30 kW water cooled arcjet[15]. The pressure ratio at the throat, however, showed a lowering trend with increasing power, a result not seen in that research.

Cold flow pressure ratios measured were higher by a factor of 1.9 to 4.6 than those predicted by 1D isentropic flow theory. During operation the pressure ratios were 4 to 10 times higher than isentropic theory (see Table 4). These ratios, or isentropic difference factors, were used for comparison in the following sections.

Performance measurements made during this research were entirely consistent with the previous data for this design. Those results will be discussed in the following section.

4.2 Performance Results

Thrust measurements for this research were taken at a lower background pressure than the pressure measurements. In the case of measurements at 35 mg/sec, this background pressure was substantially lower, around 10^{-4} vice 0.8 torr (1.9×10^{-5} vice 0.015 psi). For the higher flow rates, the background pressure was 0.15 to 0.23 torr (2.9×10^{-3} to 4.4×10^{-3} psi). The arcjet ran significantly more stable at lower pressures. Also, at 65 mg/sec, the arc voltage was observed to be 10 volts higher than under identical flow rate and current in the bell jar. The reasons for both of these observations are unknown and will require research aimed specifically at stability phenomena.

The performance data, however, were entirely consistent with the previous measurements of this arcjet design[3] (see Figures 12-15). All show linear increases in specific impulse with specific power. Efficiency tends to become lower as specific power increases, and this is mainly due to frozen flow losses. Heat used to dissociate gases cannot be converted to kinetic energy by the nozzle and is lost.

The shift in voltage observed between the bell jar and Tank 8 produced a corresponding upward shift in the specific

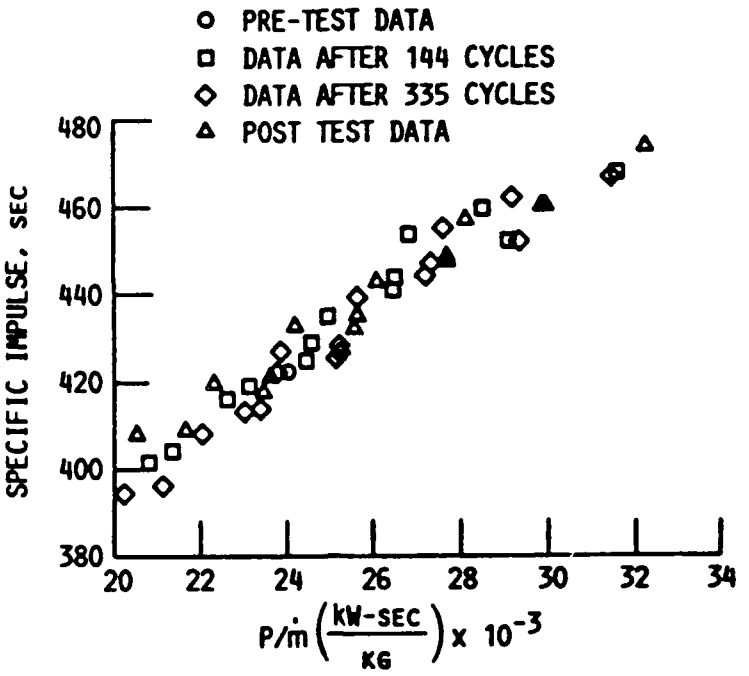

Figure 12 Previous Performance of the 1.2 kW Arcjet (from Reference 3)

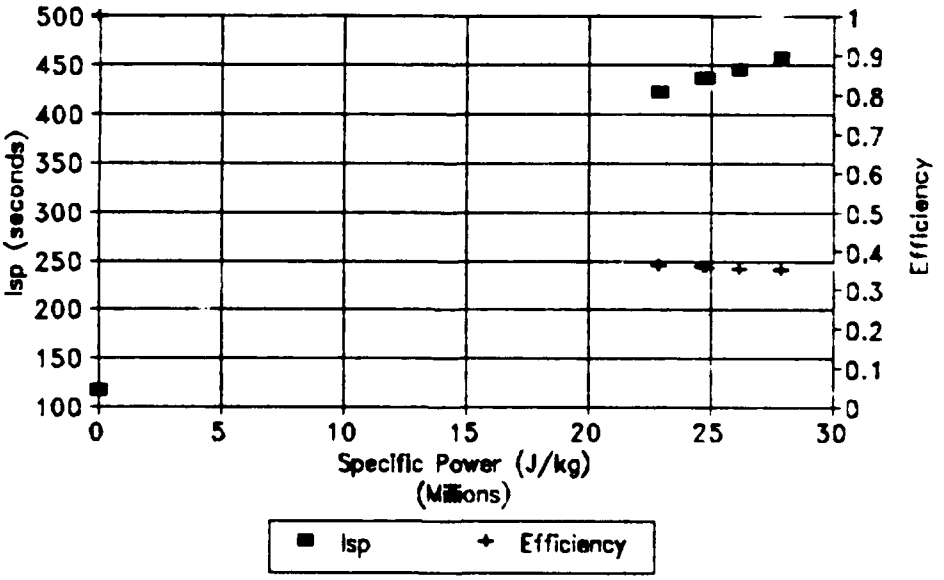

Figure 13 Specific Impulse and Efficiency vs Specific Power (35 mg/sec)

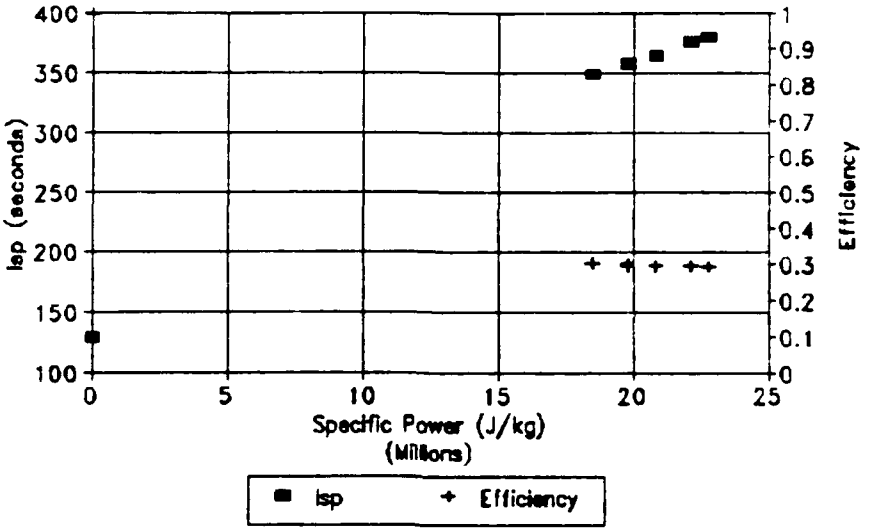

Figure 14 Specific Impulse and Efficiency vs Specific Power (50 mg/sec)

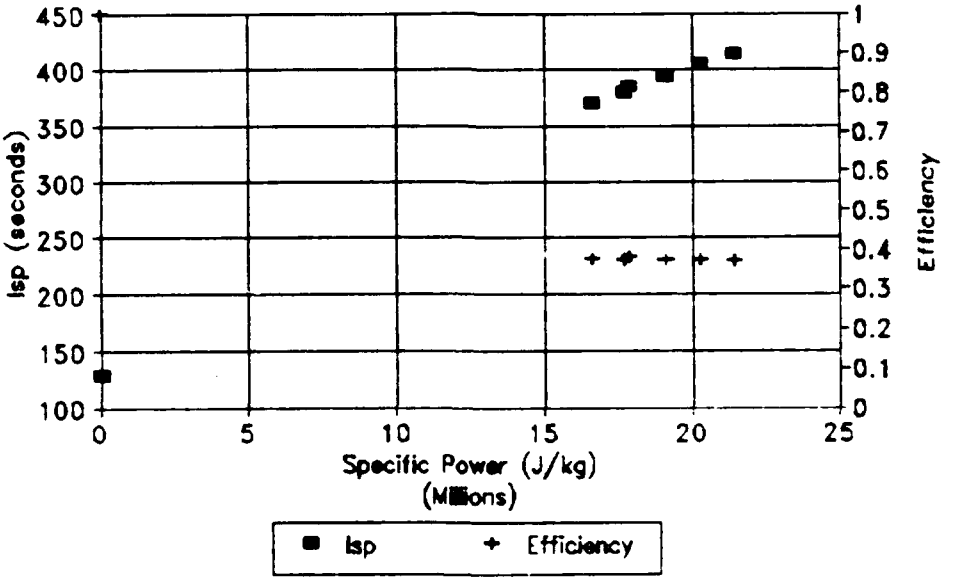

Figure 15 Specific Impulse and Efficiency vs Specific Power (65 mg/sec)

Table 4 Isentropic Difference Factors (γ = 1.4)

Tap	Cold Flow	Hot (lower)	Hot (upper)
65 mg/sec			
1/4 Tap	1.9	4.1	4.7
1/2 Tap	2.9	6.7	8.1
3/4 Tap	3.7	8.1	9.2
50 mg/sec			
1/4 Tap	2.0	4.4	4.7
1/2 Tap	3.4	6.5	6.9
3/4 Tap	4.6	9.0	9.6

power at a given arc current. However, the performance figures recorded were in excellent agreement with previous work; they were merely shifted along the specific impulse versus specific power curve. The modified arcjet was operating within the established performance parameters for this class of arcjets.

4.3 Static Pressure Results

4.3.1 Measurements at 35 mg/sec. It was at the low flow rate, 35 mg/sec, that instabilities played the largest role. Consequently, the data shows more variation than that taken at higher flow rates (see Figure 16). However, the results do demonstrate all of the major trends reported in Section 4.1.

The static pressure measured at the feed and converging taps show the characteristic linear relationship with specific power (see Figure 16). The feed pressure rise was indicative of the pressure required at the outlet of the mass flow controller to maintain a flow rate of 35 mg/sec. Due to the low Mach number in the inlet of the converging section, the static pressure measured there was actually very close to the stagnation pressure. The difference between the feed and converging tap data was due primarily to the pressure drop across the injector, but minor pressure losses from the propellant feed line and the internal propellant channels prior to the injector also contributed.

The throat data was nondimensionalized with respect to the converging section data and plotted against specific power (see Figure 17). The throat pressure ratio measured

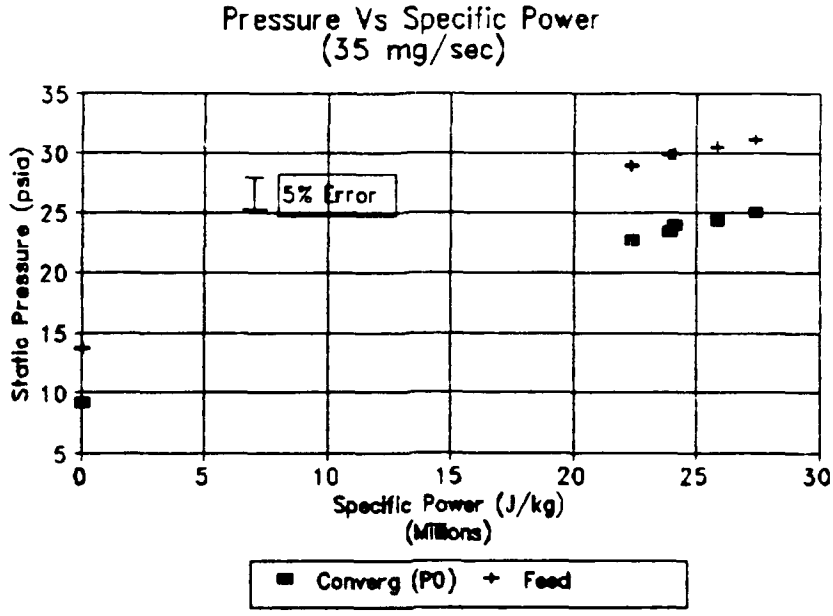

Figure 16 Feed and Converging Section vs Specific Power (35 mg/sec)

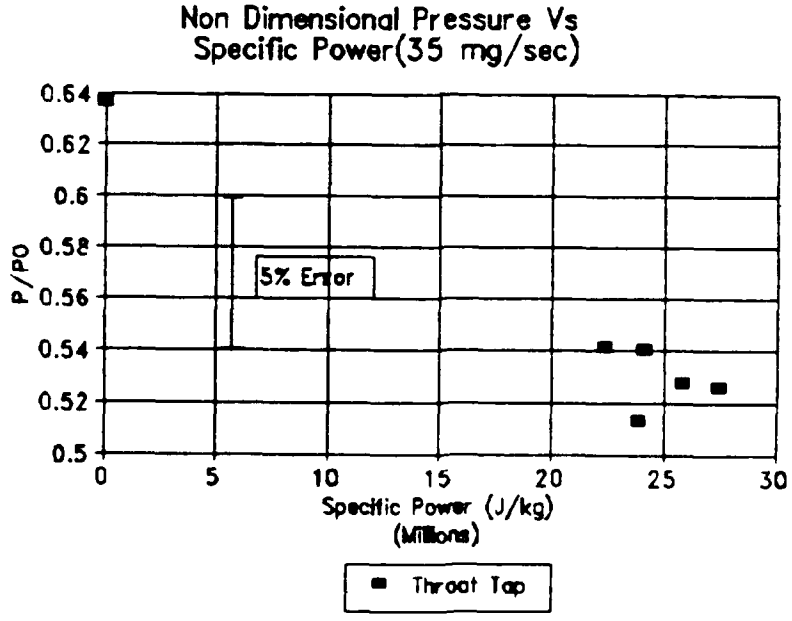

Figure 17 Throat vs Specific Power (35 mg/sec)

during cold flow was noticeably higher than that predicted by 1D isentropic theory. During arcjet operation, however, the data and isentropic theory agree quite well for a γ of 1.4. The higher ratio during cold flow could be due to the swirl induced by the injector. During operation, the viscosity of the gas increases dramatically, and the vortex may be damping out in the throat[6]. This supposition is born out by the observation of splatter marks (mostly from molten cathode material) produced in some of the previous NASA Lewis research. On a few nozzle inserts these marks exhibit a swirl pattern on the converging side while the diverging side marks are axial. However, there is still much uncertainty regarding this.

The diverging section taps all present a similar picture very much different from the throat tap (see Figures 18, 19 and 20). In the case of the 1/4 tap, the cold flow was higher than the isentropic prediction by a factor of 2.3. The hot flow at that location was higher by a factor of 4.1 to 4.6, depending upon the specific power. The discrepancy between actual and predicted static pressure for the 1/4 tap could be due to a number of things, but friction and other real gas effects are the most likely.

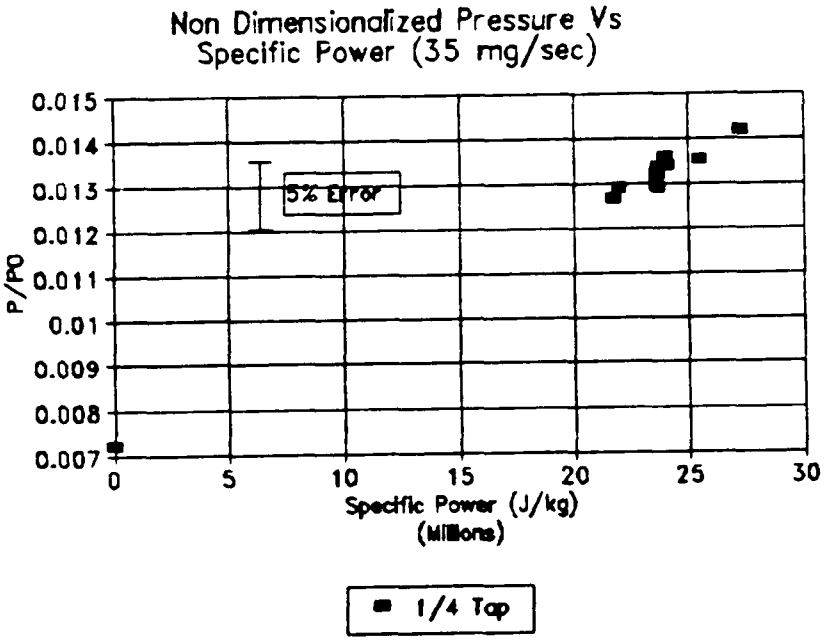

Figure 18 1/4 Tap vs Specific Power (35 mg/sec)

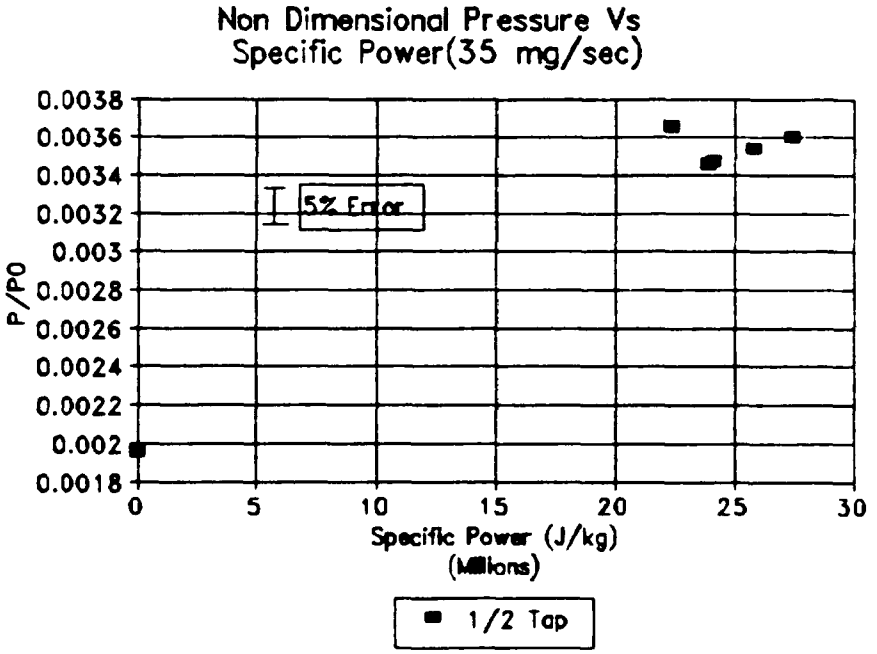

Figure 19 1/2 Tap vs Specific Power (35 mg/sec)

The 1/2 Tap data shows similar trends (see Figure 19). This data was taken from a different sample than the previous three, but was equally representative. With the exception of one point, it shows the same trend as the rest. The isentropic difference factor for cold flow was 3.8, while the hot flow ranged from 6.6 to 6.9.

The 3/4 Tap data shows significant deviation from a linear relationship (see Figure 20). While evidence of a linear increase with pressure was present, the pressure

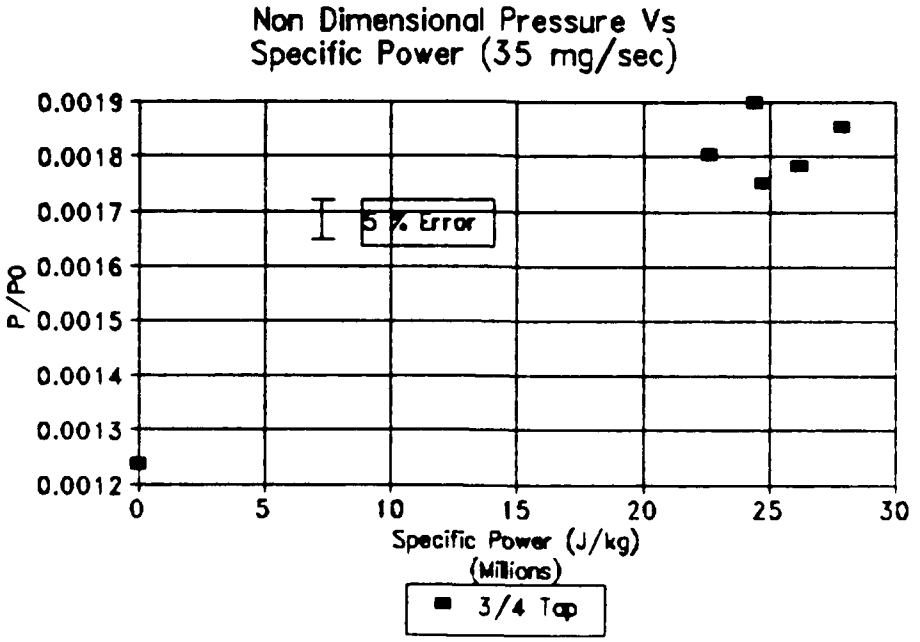

Figure 20 3/4 Tap vs Specific Power (35 mg/sec)

ratio at the lowest amperage was actually measured higher than the ratios at some higher power levels. The reason for this is unknown, and more research will be required to determine if this is some gasdynamic phenomenon or simply experimental error.

4.3.2 Pressure Measurements at 50 mg/sec. Results from the middle flow rate were very similar to those at 35 mg/sec. Representative data from several different days was graphed against specific power to demonstrate the repeatability of the measurements. In some cases a drift of approximately 10% was noticed between data taken on different days. The most likely explanation for this was minor erosion in the throat, which slightly changed the effective area ratios of the nozzle at each tap location. This hypothesis was substantiated by boroscopic examination, which shows evidence of minor erosion over the course of the testing. Fortunately, the drift stopped after approximately forty hours of operation.

The static pressure data for the feed and converging section tap were graphed against specific power (see Figure 21). There was excellent agreement between data taken on

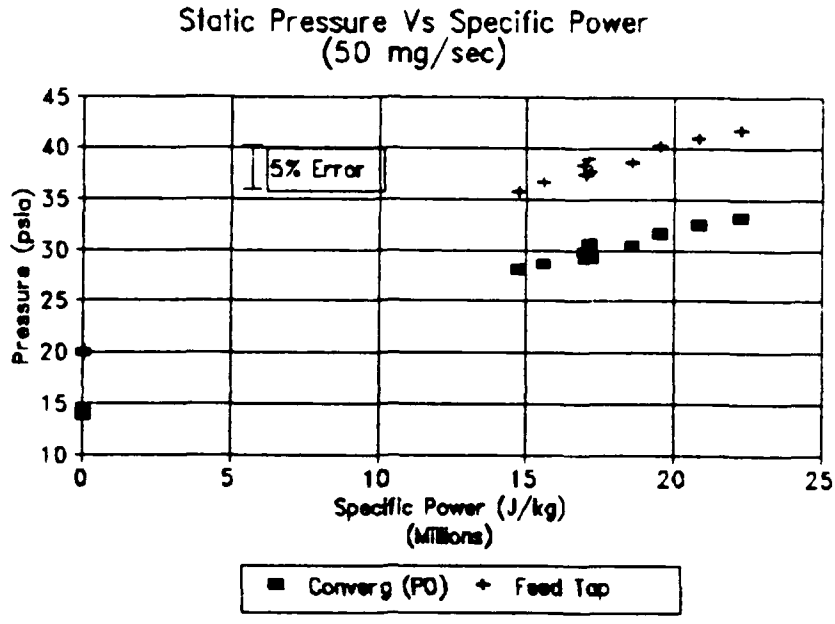

Figure 21 Feed and Converging Section Taps vs Specific Power (50 mg/sec)

two different days, approximately one week apart. A small difference in both sets was seen at a specific power of around 17 MJ/kg, which corresponds to an operating current of 11 A. Here, a slight rise was observed between measurements at the beginning of the run and at the end, several hours later.

As before, throat tap data was nondimensionalized by dividing it by the converging tap data (see Figure 22) and displayed against specific power. Again, the cold flow pressure ratio was higher than that predicted by isentropic theory, but agreed well with the same ratio measured at 35

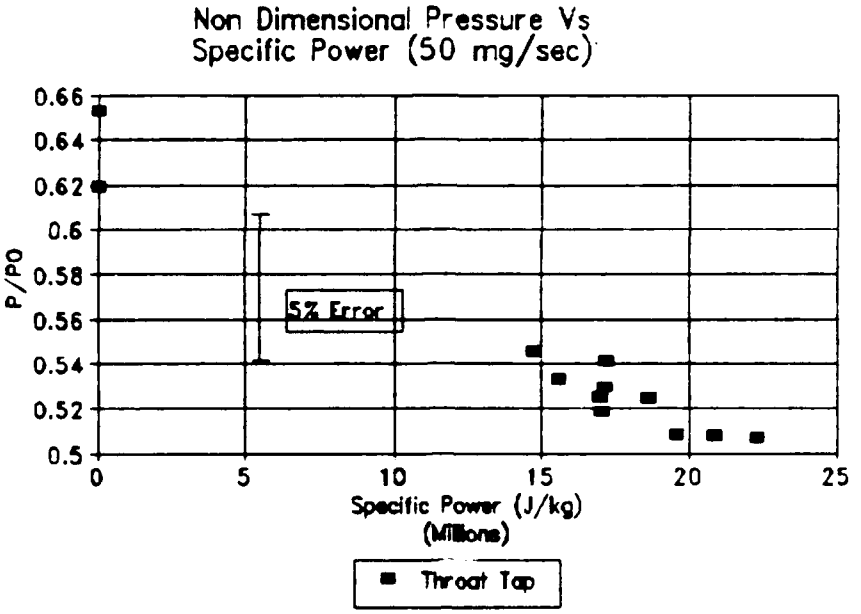

Figure 22 Throat Tap vs Specific Power (50 mg/sec)

mg/sec. The pressure ratio decreased markedly during arcjet operation, dropping below 0.5 at higher specific power levels. This suggests that perhaps some dissociation is taking place, driving γ higher and reducing the ratio. If this was the case, however, one would have expected to see this effect more strongly at the lower flow rate, where the specific power and the gas temperature is presumed to be much higher. The throat tap ratios at the low flow rate were indicative of a γ of 1.4.

Nondimensionalized 1/4 tap data was plotted against specific power in a similar manner (see Figure 23). Here,

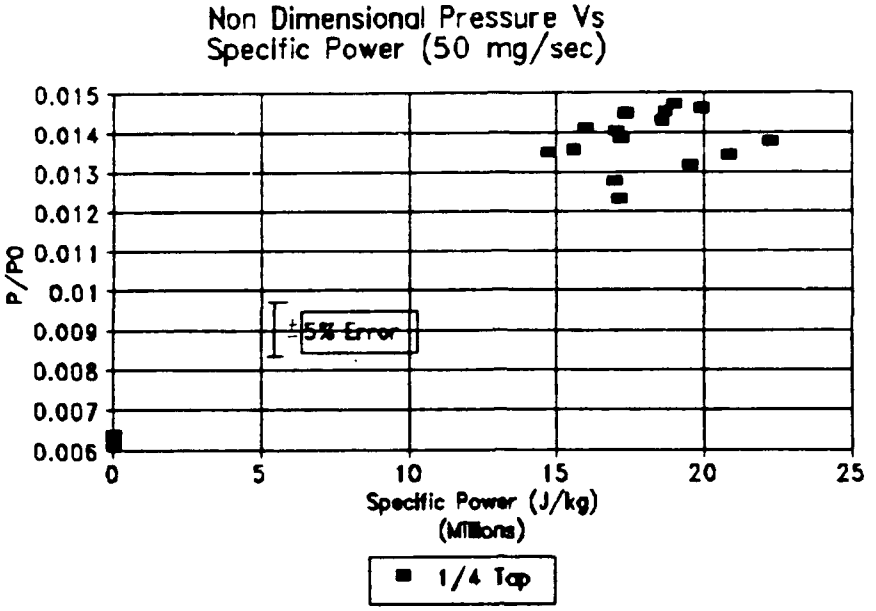

Figure 23 1/4 Tap vs Specific Power (50 mg/sec)

measurements from three different runs are presented. The drift mentioned above is particularly noticeable between the first run and two subsequent runs, which lay quite close together. For that grouping, the isentropic difference factor was 2.0. For the arcjet in operation, the difference factor varied from 4.4 at the lower powers to 4.7 at the top end. Also of note was the fact that the pressure ratios during engine operation were very similar to those at lower flow rates, in the neighborhood of 0.014, despite a difference in specific power of more than 5 MJ/kg between

the two flow rates. This suggested that pressure ratios were linked to the arc current more than to specific power.

The 1/2 tap data is presented in a similar fashion (see Figure 24). The cold flow pressure ratio seen here was slightly lower than that seen at the lower flow rate, as was the case at the 1/4 tap. Again, the operating ratios were comparable to those at the lower flow rate, but again seemed unaffected by the change in specific power. These ratios differed from the isentropic model by factors of 3.4 for cold flow, 6.5 at the low end, and 6.9 at the high end.

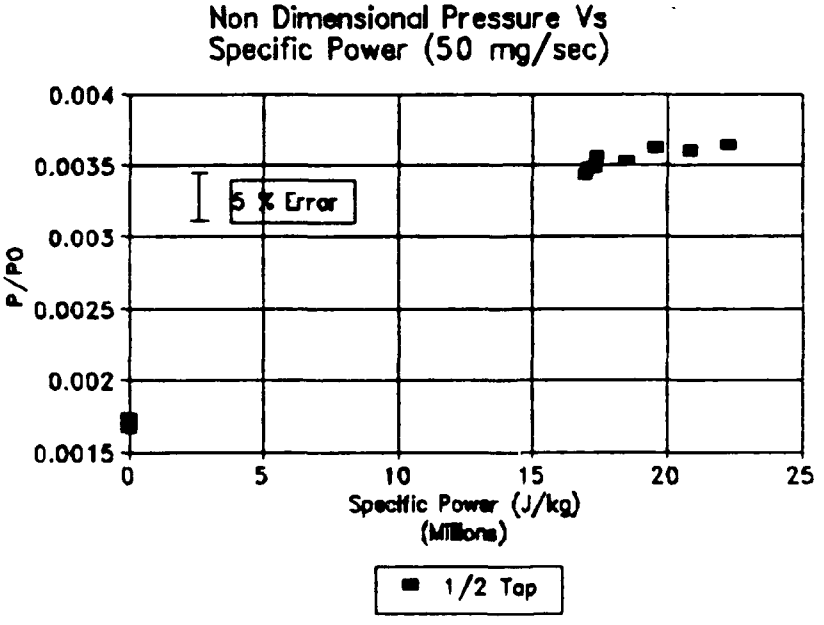

Figure 24 1/2 Tap vs Specific Power (50 mg/sec)

Finally, the pressure ratios for the 3/4 tap are plotted against specific power (see Figure 25). These ratios agree reasonably well with the lower flow rate, but are a bit higher. The isentropic difference factors at this location were 4.6 for cold flow, and 9.0 to 9.6 for the low and high ends of the specific power range for the operating arcjet.

A comparison of the difference factors for the three diverging section taps showed that the factors grew larger as the flow travelled down the nozzle. This was consistent

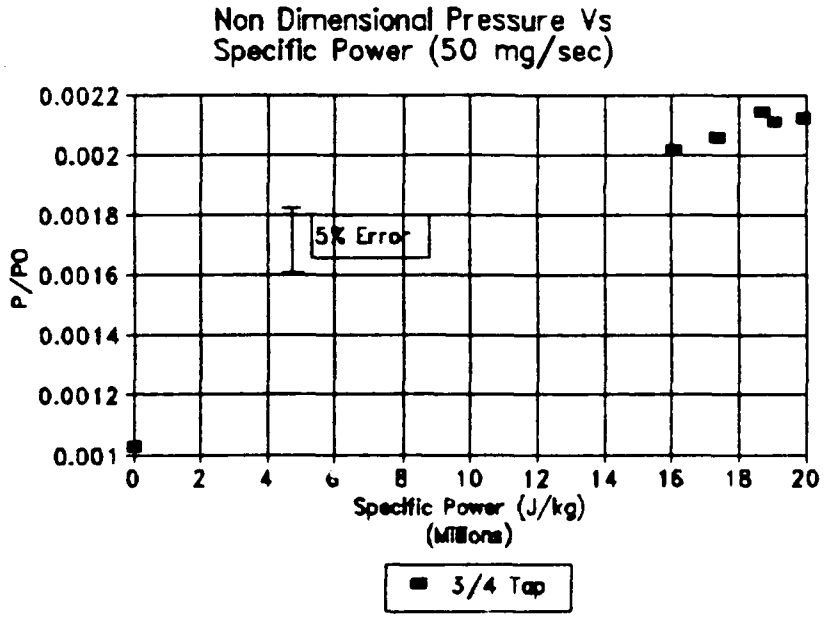

Figure 25 3/4 Tap vs Specific Power (50 mg/sec)

with the notion of a growing boundary layer in the nozzle which decreased the effective area ratio, making the pressure ratios larger by an increasing amount. This boundary layer was difficult to characterize given the severe environment in the nozzle, but one can be certain that in such a small nozzle with such high temperature gas, its effects would be large.

4.2.4 Pressure Measurements at 65 mg/sec. The best, most consistent results were obtained at the highest propellant flow rate. A rate of 65 mg/sec had not been often used at NASA Lewis in the past as the oil diffusion pumps would not operate at that mass flow. In addition, most of the power supplies available in the laboratory would not be able to produce sufficient current to meet performance goals of the development program. This flow rate, however, was well within the parameters of the standard arcjet design.

The converging section and feed pressures displayed the typical linear increase with specific power (see Figure 26). The converging pressure measured for cold flow agreed with that predicted by isentropic theory for a 2:1 molar hydrogen-nitrogen mixture flowing with a throat diameter of

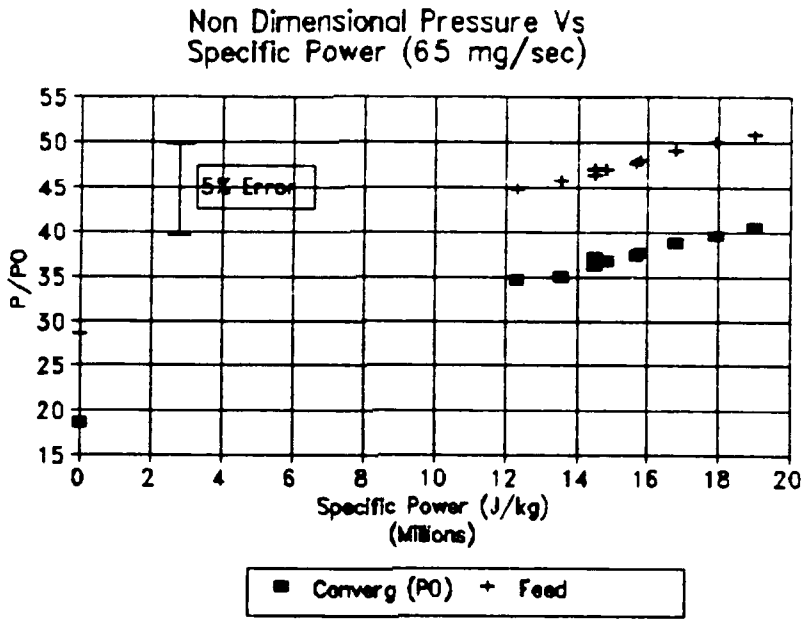

Figure 26 Converging Section and Feed Pressure vs Specific Power (65 mg/sec)

0.026 inches (6.6×10^{-4} m). This was also the case with the previous two flow rates.

Non dimensional throat data taken at this flow rate was consistent with that taken at lower flow rates (see Figure 27). The pressure ratios agree well with those taken at 50 mg/sec for both cold and hot flow. Again, the ratios dipped below that predicted by isentropic flow with a γ of 1.4, suggesting that some dissociation was taking place. In this case one would expect that the ratios measured at the low flow rates, with correspondingly higher specific powers, would tend to dissociate more, especially since the absolute

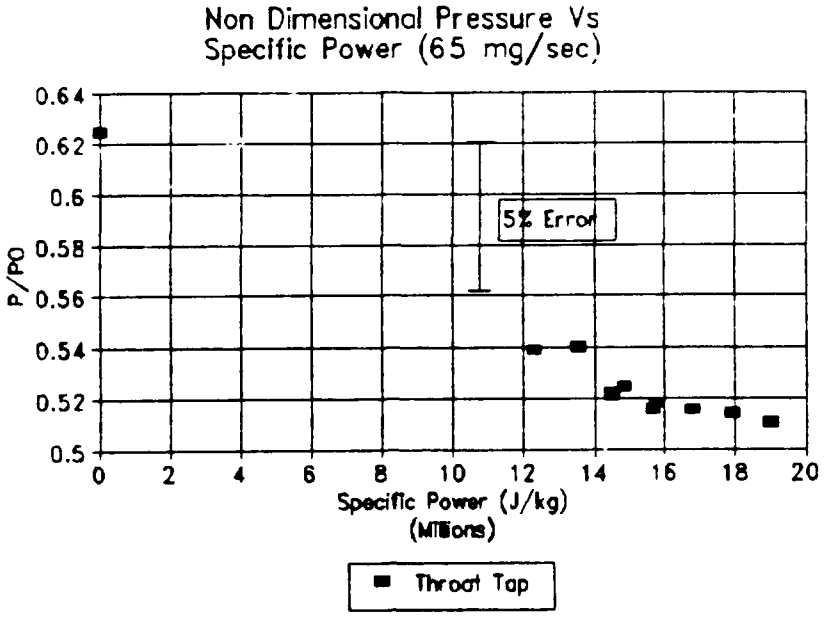

Figure 27 Throat Tap vs Specific Power (65 mg/sec)

pressure was lower in those situations. There was no clear evidence of such a trend in this data, however. Again, the ratios at the throat seemed to depend more on arc current than specific power. This hypothesis would account for the similarity between the ratios, which were taken over the same range of arc currents but with largely different specific powers.

Pressure ratios from the 1/4 tap were plotted against specific power in Figure 28. Here some drift was noticeable between two different runs, but were within the previously noted repeatability of ±5%. The difference factors were 1.9

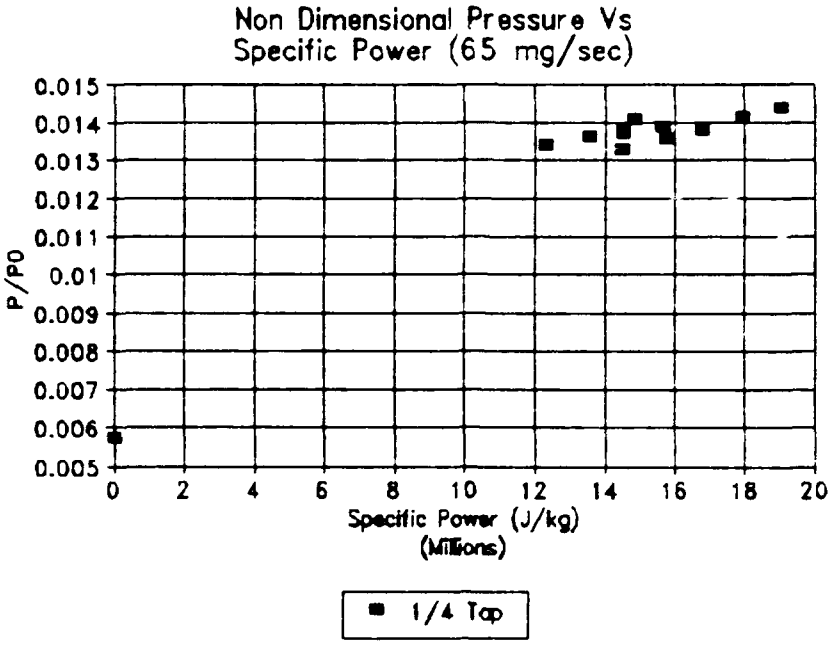

Figure 28 1/4 Tap vs Specific Power (65 mg/sec)

for cold flow, and from 4.1 to 4.7 over the operational range of the arcjet. The data compared well with ratios taken at lower flow rates.

Measurements taken at the 1/2 tap at this flow rate were similar (see Figure 29). The data were very linear with specific power. The ratios were slightly higher than at either of the two lower flow rates, but in the same region. The isentropic difference factors at this tap location were 2.9 for cold flow, and varied from 6.7 to 7.7 over the operating range of the arcjet.

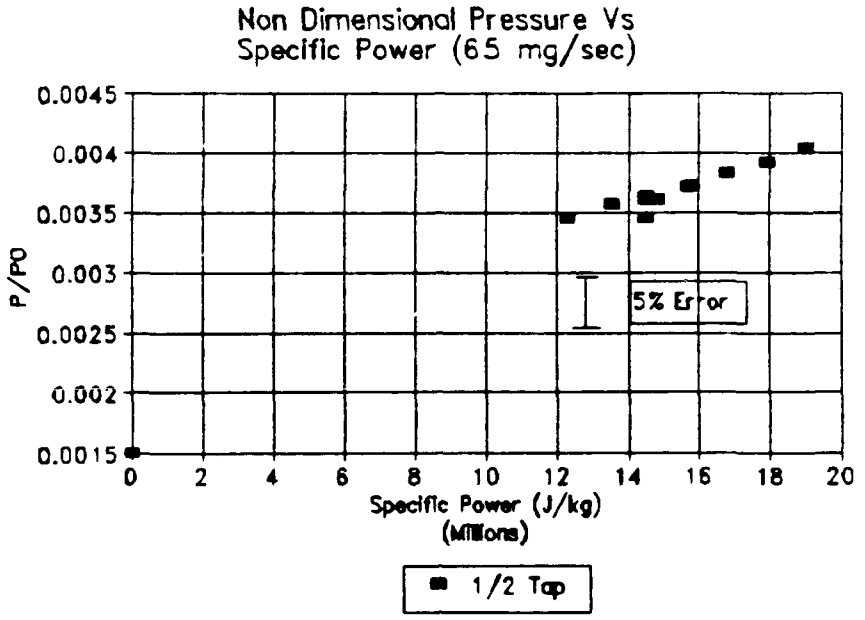

Figure 29 1/2 Tap vs Specific Power (65 mg/sec)

Finally, the measurements from the 3/4 tap were plotted against specific power (see Figure 30). Again, the ratios were in excellent agreement with those measured at 50 mg/sec. The isentropic difference factors continued to grow, with a cold flow difference factor of 3.7, and hot flow factors between 8.1 and 9.2. When compared with difference factors from 50 mg/sec, the difference factors at high flow rate were uniformly lower. This agreed with the notion that the differences were influenced by boundary layer growth, as at a higher density the boundary layer thickness would tend to be smaller. It must be stressed

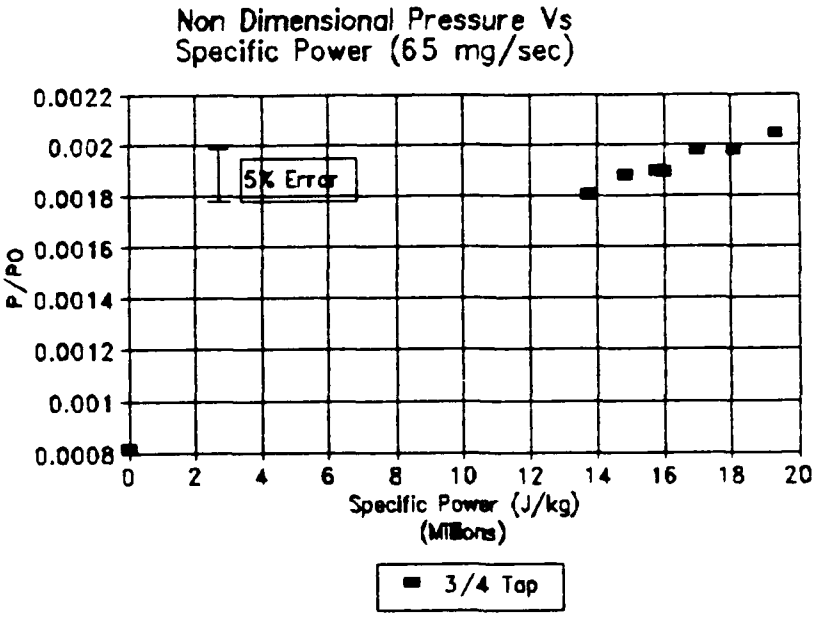

Figure 30 3/4 Tap vs Specific Power (65 mg/sec)

again, however, that characterization of the boundary layer in this case is very difficult, and these analogies are meant to demonstrate trends only.

4.2.5 Comparison of Data with a Simple Thermodynamic Model. Diverging section data at a flow rate of 65 mg/sec was compared with results from the 1D thermodynamic model developed in Section 2.2 (see Figures 31,32, and 33). All three showed that the model overpredicted the actual hot flow pressure ratios by a factor of around two. The slope of the model, however, fit the data remarkably well, as the

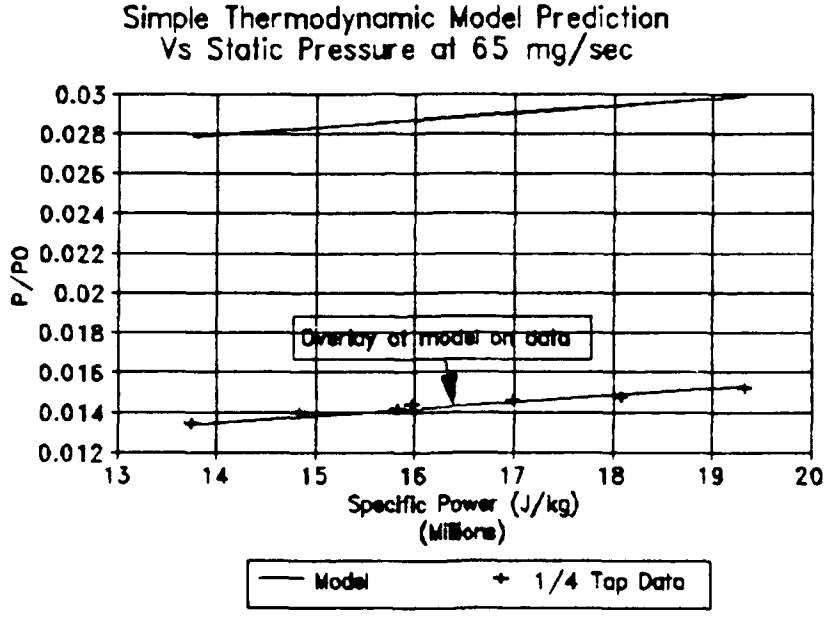

Figure 31 Comparison of 1/4 Tap Data with Model

overlays of the model onto the data demonstrated. The slope of the model was driven by many factors: the estimated specific heat at constant pressure C_p, the compressibility factor K, and the slope of the ratio of exit velocities obtained from performance data. The values of these parameters, or at least the product of these parameters, seems to match the data very well.

The actual values predicted by the model, however, matched the experimental data poorly. Considering the coarseness of the analysis, though, a factor of two correspondence was acceptable. In reality there are sharp

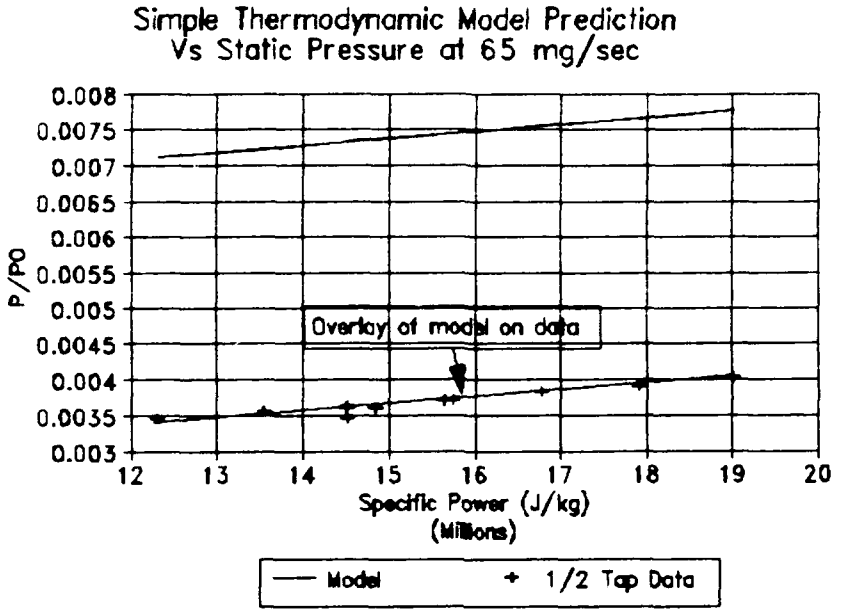

Figure 32 Comparison of 1/2 Tap Data with Model

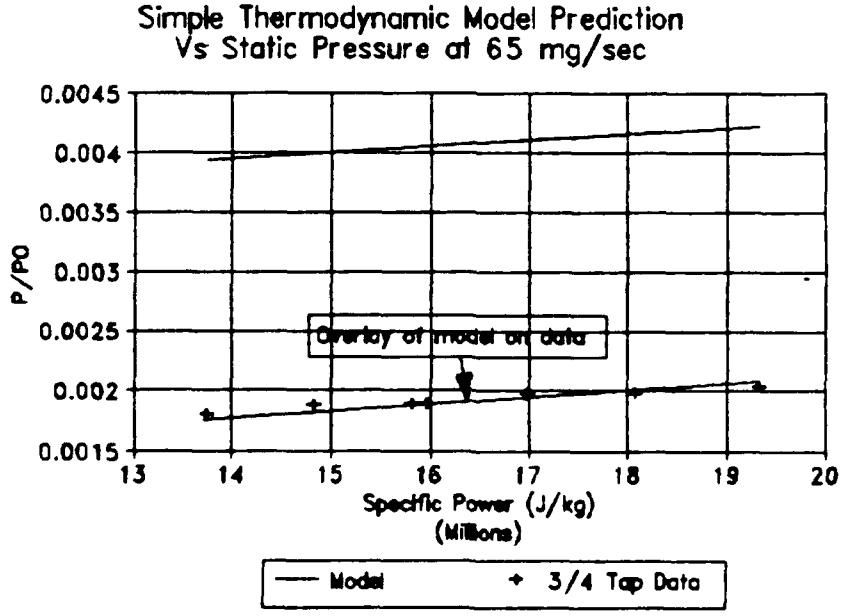

Figure 33 Comparison of 3/4 Tap Data with Model

radial profiles in velocity, temperature and composition, and this method smoothed them into uniform profiles. It was not surprising, therefore, that major differences did exist between this very simple model and experimental measurements. In light of the fact that there were no accurate computational models for arcjet pressure profiles, the thermodynamic model served quite well as a comparison, if nothing else.

V Conclusions and Recommendations

5.1 Conclusions

In order to establish data taken from the modified arcjet as meaningful in the context of previous NASA LeRC low power arcjet research it was necessary to compare the performance characteristics obtained during this research with that recorded earlier. The discussion in Section 4.2 showed that the test article performed well within the established specific impulse and efficiency ranges for arcjets of this general design. It is not unreasonable to conclude, then, that the static pressure data collected applies to the LeRC low power arcjet with reasonable accuracy.

All static pressure data recorded was repeatable to within ±5%. With the exception of throat data, the trends observed confirmed previous work with high power, water-cooled arcjets[15]. In that instance there was substantial deviation from the previous work. Whereas Harris et al reported a positive sloped linear dependance of the static to stagnation pressure ratio at the throat, no such trend

was observed in this research. Nozzle geometry and wall cooling conditions, which differed substantially, between Harris' work and this, are the most likely sources for this disagreement. Data in this research suggested that perhaps the swirl in the flow caused by the injector was being damped out before reaching the throat during arcjet operation.

Diverging section tap data showed a linear dependance with specific power. A comparison of this data with isentropic predictions for the nozzle suggested the presence of a growing boundary layer in the nozzle. It must be stressed, however, that characterization of the boundary layer in this nozzle would be impossible without much more information about the flow conditions.

A simple thermodynamic model was also used as a comparison for the diverging section pressure data. The model significantly overpredicted the pressure but showed excellent agreement in slope with the recorded data. The most likely explanation for agreement in slope is that performance data dominated the slope of the model. That would indicate a definite correlation between thrust and static pressure along the nozzle.

5.2 Recommendations

A number of unknowns were uncovered during the course of this investigation. The chief enigma was the question of why this particular test article, identical in geometry to several previous models, should have operated so unstably while this was never a problem in the past. It was difficult to imagine that the one piece construction of the forward housing was the cause; rather, it may have had something to do with the method of construction. A similar piece machined without the nozzle should be ordered. It can then be machined to more severe specifications by the NASA Lewis machine shop than was this one, which was finished by the supplier. A repeat investigation could reduce instabilities at the lower flow rates. Also, a similar investigation for radiation cooled high power arcjets needs to be done.

The issues of boundary layer growth and exact propellant composition in the nozzle came up repeatedly during the discussion. With only pressure, power, and performance data to analyze, characterization of these properties was extremely difficult. Due to the small

geometries and harsh environment inside arcjets, such data would be difficult to get. Considering the potential value of that knowledge, the effort would be well spent.

Computational models need nozzle wall temperature profiles for validation as well as pressure data. It would also be useful to get measurements of the nozzle wall temperature during operation. This would be very difficult to do, but perhaps high temperature thermocouples could be placed inside guide holes similar to those used in this experiment to place pressure taps. An accurate internal wall temperature profile could then be combined with pressure data so that an analysis of the heat transfer between the anode wall and the gas could be done. Finally, the effort to develop a computational model for arcjets should continue. Experimental profiles of temperature and pressure along the nozzle will be necessary to verify them. As it stands, developmental engineering in the field is chiefly empirical, and thus expensive. The ability to accurately predict performance and other characteristics of arcjets without lengthy laboratory tests would shorten the development cycle considerably and make the widespread use of arcjets for spacecraft applications a reality that much sooner.

Appendix A: Arcjet Construction

The design of the NASA Lewis 1.2 kW arcjet can be divided into two major subassemblies: the rear housing and the forward housing assembly (see Figure 2, page 11). In general, the rear housing is a hollow tube of boron nitride through which the cathode is passed. Its major functions are to serve as an anchor for the cathode, to keep the cathode well insulated to avoid shorts, to channel propellant forward toward the nozzle, and finally to provide the structural compression necessary to keep the entire arcjet together. The very end of the rear housing is capped with a pressure fitting that not only seals that end but serves to hold the cathode precisely in place when tightened. Another pressure fitting to the side, about half way up the housing, is connected with the propellant feed line and channels the gas through to the hollow core of the housing. Inside this core the cathode is surrounded by three loosely fitting objects: an Inconel spring, a boron nitride plunger, and an alumina tube. When assembled with the forward housing assembly, the spring and plunger compress the pieces of the forward housing, holding them firmly in place. The alumina tube slides in between the

cathode and the plunger, and prevents any potential arcing at the seam between the plunger and the front insulator.

The major functions of the forward housing assembly are simply to inject the propellant into the arc gap and eject it out of a nozzle. It is basically a hollow tube of molybdenum--the forward housing--through the front end of which a nozzle insert of 2% thoriated tungsten is fitted. Together these two pieces comprise the anode. The nozzles come in either of two designs, a 2.5 or 5% taper fit and a flange fit (see Figure 3, page 13). The flange fit requires two Grafoil (graphite foil) gaskets to make a seal. Immediately to the rear of the nozzle insert is a molybdenum injection disk, followed by the front insulator. Propellant flows forward in grooves in the front insulator, enters notches in the outside of the injector disk, and is channeled through 0.010 inch tubes to be injected tangentially around the tip of the cathode. Grafoil seals are also placed between the front insulator and the injector, and the injector and the nozzle insert to insure that the gas does not leak around the injector and directly into the nozzle. The forward insulator runs the length of the forward housing, is grooved to provide flow for the propellant, and is composed of boron nitride.

The two major subassemblies are held together by two molybdenum flanges through which four 10-32 x 4 inch screws are passed. These screws are carefully tightened to prevent damage to the cathode and the surrounding insulating material. Following this, a micrometer is used to set the arc gap to 0.024 inches.

Appendix B: Test Article Construction

To accommodate pressure measurements in the nozzle, taps were bored into the one piece forward housing. This was accomplished by first drilling guide holes 0.125 in. in diameter radially in from the edge of the housing until they were within 0.1 in. of the nozzle. The actual tap diameter specified as 0.006 - 0.010 inches, was drilled from guide holes to the nozzle using electron discharge machining, or EDM. These EDM techniques led to very clean, sharp tap holes as microphotographs of the outer two taps show (see Figure 34). These photographs also demonstrated that the taps were within specifications and were typically 0.007 inches in diameter. It was not possible to make photographic measurement of the throat and converging section taps.

Once the taps had been drilled, 0.126 inch molybdenum tubes were then interference fitted into the 0.125 inch guide holes, providing a tight seal. Testing of this method had been done prior to actual modification using a 2% thoriated tungsten slug and 1/8 in tantalum tubing. After some trial and error, the method passed a helium leak check[22]. Molybdenum was chosen for the test article instead

of tantalum because it has similar properties and is less costly. Once the forward housing with the pressure tap tubes installed was assembled into an arcjet, however, some minor leaking was detected around the converging and throat taps during a 100 psi nitrogen leak check. The amount leaking was judged to be less than that which normally leaks from the various gas fittings in the arcjet and so was deemed acceptable. Moreover, the relative thermal expansion coefficients of tungsten and molybdenum ensure that this fit would get much tighter as the housing heats up to operating temperature, around 900 C.

Five taps were drilled: one in the converging section, one in the throat (or constrictor), and three in the diverging section. Exact location of these taps was difficult to determine. Two methods were tried, microphotography and direct micrometer measurement of a microscope focal plane.

Microphotography consisted of taking Polaroid photographs at known magnification and measuring the apparent diameter of the nozzle at the location of each tap. While this produced good qualitative results (such as determining that the tap exits were free of burrs and other obstructions) comparison of these pictures with known

lengths, namely the diameters of the throat and exit plane, showed that there was too much error in this method to give good results. Diameters of the throat and exit plane were confirmed by direct measurement of a mold of the nozzle. This method was used only to locate the converging section tap, as the length of the forward housing made measurement by the second method impossible. In this case, the photograph was scaled by the apparent diameter of the throat in the picture. Since the important parameter from a gasdynamic standpoint is the area ratio, this method did not seem unreasonable. The axial location was then determined by assuming the converging section was a perfect cone with a 30° half angle, truncated at the diameter of the throat.

The diverging section taps, however, were measured by a microscope whose vertical position was recorded by a dial micrometer. By zeroing the micrometer at the forward end of the housing (which formed the exit plane of the nozzle) and then focusing on the top of a 0.006 inch wire projecting from each of the three diverging section taps, the tap's distance from the exit plane can be measured. The accuracy of the method is estimated to be about ±0.010 inches, based

on the microscope operator's subjective determination of what position is "focused."

The location of the throat tap can only be quantified by saying that it is in the constrictor, between 0.481 and 0.491 inches from the exit plane. This was determined by photomicrograph and various visual examinations. The intended location of this tap was to have been 0.470 in. well outside the constrictor but still quite close, so as to measure conditions near the throat without disturbing the flow there. However, EDM bores can drift, and the tap entered the nozzle squarely in the constrictor.

Appendix C: Strip Chart Data

Three representative strip charts, one for each flow rate, have been included (see Figures 34, 35, and 37). The typical stability phenomena observed throughout the research are readily seen in these recordings.

In all three cases, the top trace represents the 1/4 tap pressure measured relative to the bell jar's background pressure, while the bottom trace is the arc voltage. Periods of instability are marked by large variations in both voltage and pressure. This is particularly visible in Figure 34, which was recorded during arcjet operation at a mass flow rate of 35 mg/sec.

Stability trends can also be discerned from these figures. There is marked progression toward steady operation as the flow rate increases. As the flow rate increases the disturbances are smaller and more widely spaced.

Arc current also has a strong influence on stability. In particular, see Figure 35. The step change in arc current between 9 A and 12 A produces a clear improvement in stability.

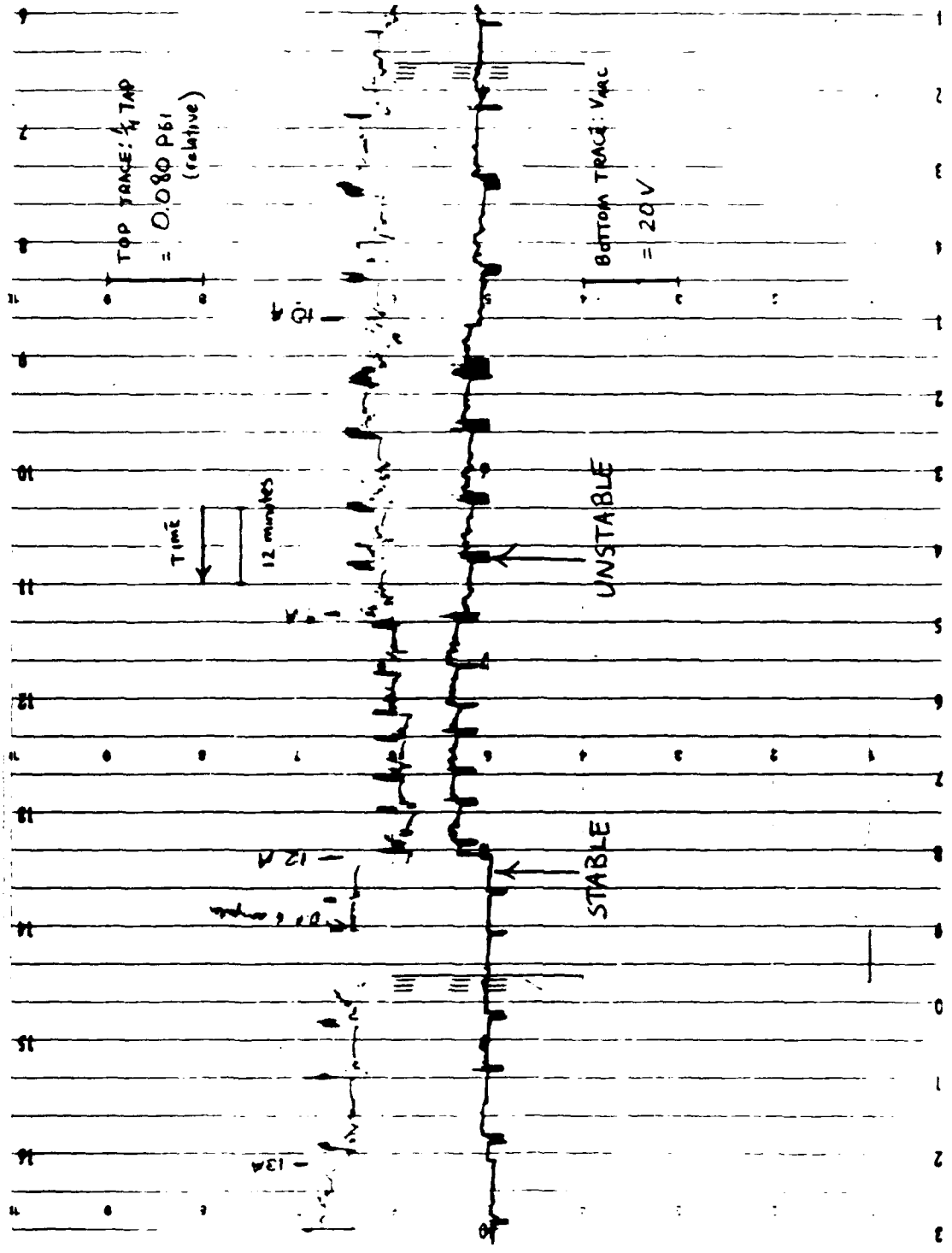

Figure 35 Stripchart Trace of Arcjet Operation at 50 mg/sec

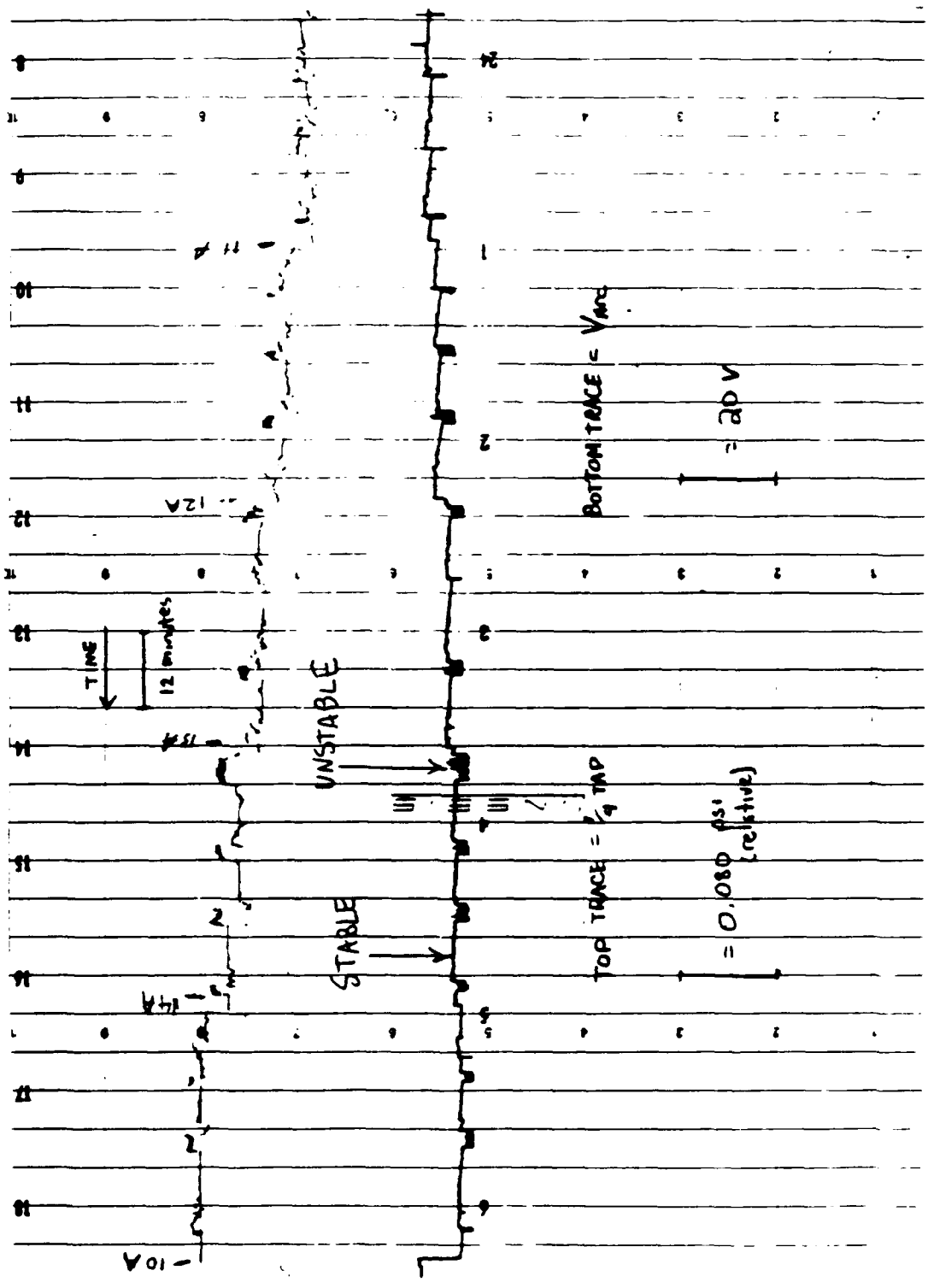

Figure 36 Stripchart Trace of Arcjet Operation at 65 mg/sec

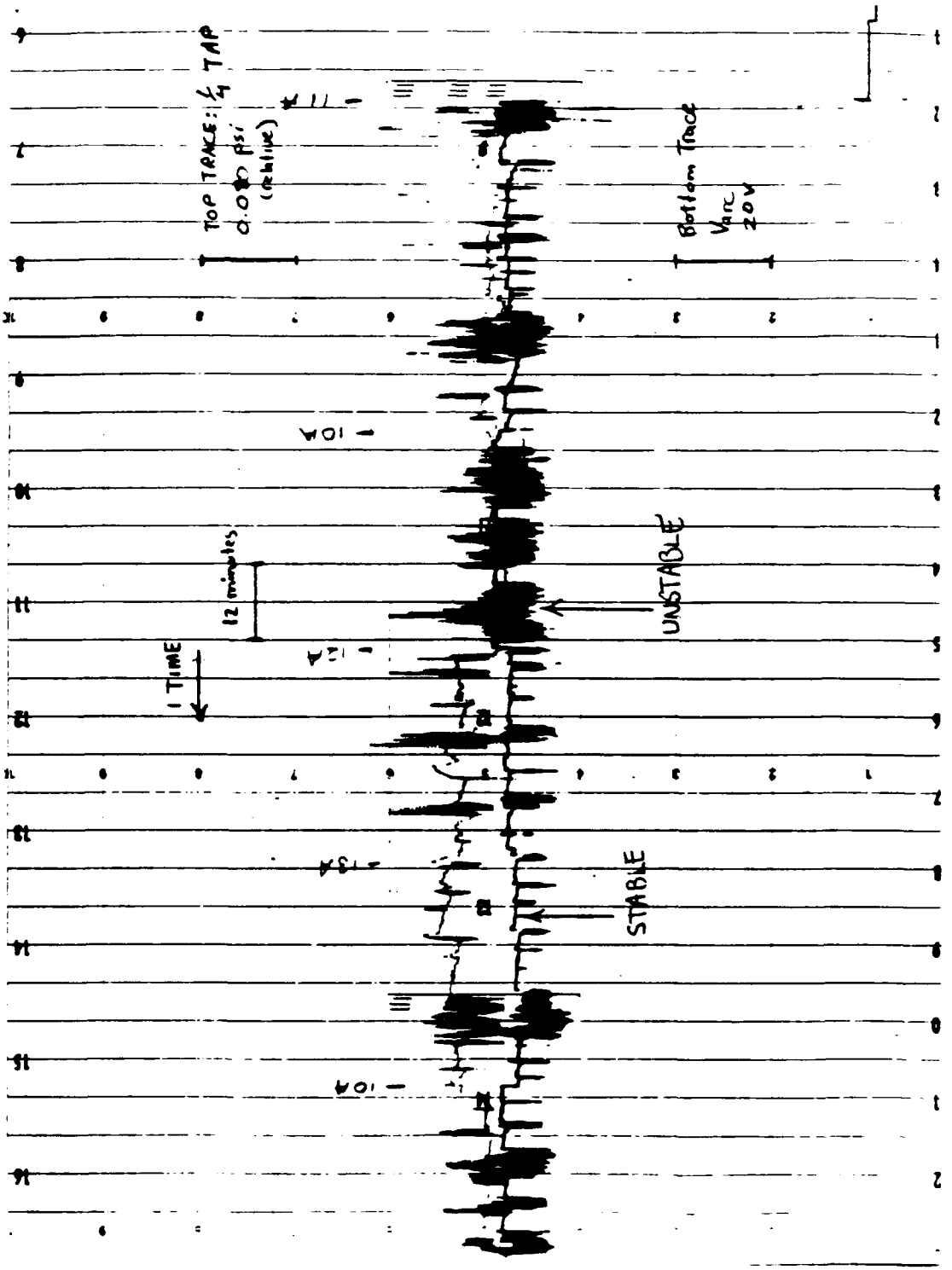

Figure 37 Stripchart Trace of Arcjet Operation at 35 mg/sec

Bibliography

1. Jahn, R.G., Physics of Electric Propulsion, McGraw-Hill, New York, NY, 1968.

2. Planeaux, J. Class notes from MENG 632 Non Chemical Propulsion, School of Engineering, Air Force Institute of Technology, Spring 1991.

3. Curran, Francis M. and Thomas W. Haag, "An Extended Life and Performance Test of a Low Power Arcjet," Proceedings of the AIAA/ASME/SAE/ASEE 24th Joint Propulsion Conference, AIAA-88-3106 (NASA TM 100942), Boston, MA, 1988.

4. Morren, Earl. Private communication, Cleveland OH, August 1991.

5. Sankovic, J.M. Private communication, Cleveland, OH, July 1991.

6. Sarmiento, Charles J. Private communication, Cleveland, OH, August 1991.

7. Sutton, George P. and Donald M. Ross. Rocket Propulsion Elements (Fourth Edition), John Wiley and Sons, New York, 1976.

8. Curran, Francis M, David H. Manzella and Eric J. Pencil, "Performance Characterization of a Segmented Anode Arcjet Thruster," Proceedings of the 21st International Electrical Propulsion Conference, AIAA-90-2582 (NASA TM 103227), Orlando, FL, July 1990.

9. -----, and David H. Manzella, "The Effect of Electrode Configuration on Arcjet Performance," NASA TM 102348, Cleveland, OH, July 1989.

10. -----, Amy J. Sovie and Thomas W. Haag, "Arcjet Nozzle Design Impacts," NASA TM 102050, Cleveland, OH, 1989.

11. Sankovic, John M. "Investigation of the Arcjet Plume in Near Field Using Electrostatic Probes," NASA TM 103638 Cleveland, OH, 1990.

12. Zana, Lynette M. "Langmuir Probe Surveys of an Arcjet Exhaust," Proceedings of the AIAA/SAE/ASME/ASEE 23rd Joint Propulsion Conference, AIAA-87-1950 (NASA TM 89924), San Diego, CA, June 1987.

13. Manzella, David H, Francis M. Curran, et al "Preliminary Plume Characteristics of an Arcjet Thruster," Proceedings of the AIAA/DGLR/JSASS 21st International Electric Propulsion Conference, AIAA-90-2645, Orlando, FL, July 1990.

14. Curran, Francis M., S. Ray Bullock, et al "Medium Power Hydrogen Arcjet Operation," Proceedings of the AIAA/SAE/ASME/ASEE 27th Joint Propulsion Conference, AIAA-91-2227, Sacramento CA, June 1991.

15. Harris, W.J., E.A. O'Hair, L.L. Hatfield et al, "Static Pressure Measurements in a 30 kWe Class Arcjet," Proceedings of the AIAA/SAE/ASME/ASEE 27th Joint Propulsion Conference, AIAA 91-2457, Sacramento, CA, June 1991.

16. Shapiro, Ascher H., The Dynamics and Thermodynamics of Compressible Fluid Flow, (Reprint Edition), Robert E. Krieger Publishing Company, Malabar, FL, 1983.

17. Hasen, Gerald A. Course notes from AERO 622, Introductory Hypersonics, School of Engineering, Air Force Institute of Technology, Winter, 1991.

18. Anderson, John D. Hypersonic and High Temperature Gas Dynamics, McGraw-Hill, New York, NY, 1989.

19. Endevco, General Catalog, Endevco, San Juan Capistrano, CA, 1989.

20. Sarmiento, Charles J., and Robert P. Gruber, "Low Power Arcjet Thruster Pulse Ignition," Proceedings of the AIAA/ASME/SAE/ASEE 23rd Joint Propulsion Conference, AIAA-87-1951 (NASA TM 100123), San Diego, CA, June 1987.

21. Haag, Thomas W. and Frank M. Curran, "Arcjet Starting Reliability: A Multistart Test on Hydrogen/Nitrogen Mixtures," Proceedings of the 19th International Electric Propulsion Conference, AIAA-87-1061 (NASA TM 89867), Colorado Springs, CO, May 1987.

22. Curran, Frank M., Private Communication, Cleveland, OH. April 1991.